Chapter 2

α-Hydroxy acids modified β-cyclodextrin capped Iron Nanocatalyst for rapid reduction of nitroaromatics: a sonochemical approach

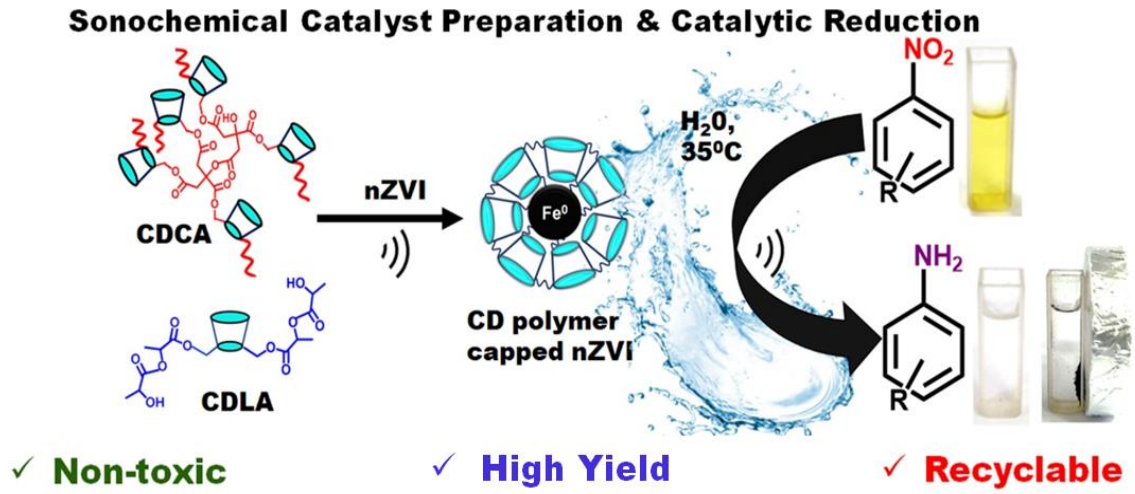

Published in *International Journal of Biological Macromolecule*, 2022, 209, 1504-1515

2.1 Introduction

Nano-engineered catalysts magnetic nanoparticles have been of major interest to researchers in area of catalysis owing to its ability to heterogenize the nanoparticles in addition to providing ease of catalyst separation via magnetic decantation. In the class of magnetic nanoparticles, specifically iron oxide nanoparticles have been widely explored for various applications such as catalysis, drug delivery, adsorption etc [1][2][3]. Recently it is reported that iron is considered as "metal with minimum safety concern" by regulatory authorities[4].

Besides iron oxide nanoparticles, elemental zerovalent iron existing in a bcc crystal structure as alpha-Fe has very reactive surface sites in its nano state. Elemental zerovalent iron nanoparticles (nZVI) have been the subject of considerable research as they can play vital role in aiding greener synthesis, minimizing environmental contaminants, sustainable catalysis. They are earth abundant, non-toxic, biocompatible, adorned with excellent electron donating capability and have high potential to behave as catalysts[5]. In this regard, an excellent opportunity come into light for application of nZVI in the field of catalysis. Excellent catalytic activity of iron nanoparticles in zero valent state (nZVI) has been reported for few reactions like Fenton process as well as for dehalogenation of aromatic halides[6]. They can be synthesized at ease and demonstrate large surface to volume ratio. For the synthesis of zerovalent iron nanoparticles, a significant amount of research has been done and well documented so far.[7] The physical methods for preparation of nZVI are not cost effective and chemical methods are simple due to homogeneity and ease of operation.

Although the emergence of zerovalent iron nanoparticles is rapidly progressing due to its various advantages but they associated with various factors such as high aggregation rate, surface oxidation and interaction with the environment are the limitations responsible for hindering the full-fledged catalytic application of these nanoparticles. To circumvent these problems, various strategies have been utilized to enhance the stability of nZVI. For instance modifying nanoparticle surface by functionalization with moieties viz. cyclodextrin[8], chitosan[9], starch[10], cellulose[11], polyphenols[12], riboflavin[13], organic acids (citric acid)[14]etc. Other approaches include modifying viscosity (using guar gum, xanthan gum etc.), incorporating a supporter (carbon porous material, biochar etc.)[15][16][17], using protective coatings (e.g., clay)[18][19].

Amongst these, β-Cyclodextrin, a well-known host for hydrophobic substrates and multiple

hydroxy groups can aid in capping the nZVI to act as catalyst. Recently, Krawczyk *et al*. have made the first attempt to demonstrate the catalytic application of β-cyclodextrin functionalized nZVI for the reduction of 4-nitrophenol to 4-aminophenol[8]. However, due to solubility in water, the β-CD capping may not be efficient which hampers the recycling ability of the catalyst. Since very little work is focused on recycling of nZVI based catalyst, it would be interesting to functionalize with environmentally friendly crosslinked polymers as they are endowed with various functionalities like –OH, $–NH_2$, –SH, –COOH to stabilize the metal nanoparticles via ionic interaction. β-CD derived crosslinked polymers can be ideal stabilizing agents due to stable, biodegradable and amphiphilic nature[20][21][1]. They can facilitate reactions in aqueous medium in less time and with high recyclability. Such β-CD derived crosslinked polymers capped nZVI have not been explored for catalytic applications of nitroaromatics, to the best of our knowledge. There has been a recent advent in the usage of sonochemical approach for the synthesis and catalytic application.

Sonochemical approach is associated with employing ultrasound waves having frequency in the range of 20 kHz - 2 MHz in order to facilitate chemical, thermal and physical effects in solution[22]. These effects result in generation of intense local heat increasing the solution temperature to ~5,000 K and high pressure ~1,000 bar. These elevated temperature and pressure conditions result in the phenomenon of acoustic cavitation and cage effect causing an acceleration in the reaction rates assisting reaction completion in shorter time under milder conditions with high yield[23][24]. These factors make sonochemical approach more convenient, fast, simple and easily controlled as compared to conventional methods. Therefore, this unique technique can be utilized for green, economical and environmentally-friendly approach for both synthesis as well as application of the engineered nanocatalysts[25][26][27][28][29].

This is owing to the fact that rationally synthesized nanocatalysts are designed to have enhanced catalytic activity and selectivity towards chemical processes under study.

The reduction of nitroaromatics is an industrially important process as the products, aromatic amines, are versatile intermediates and precursors which are further used in pharmaceuticals, agrochemicals, dyes and polymers[30][31][32].

The ultimate goal was to synthesize crosslinked polymers derived from renewable resources, utilizing them for capping very unstable zerovalent iron nanoparticles and then employing the

resulting material as nanocatalysts having the following features:

1. Sonochemical synthesis of stable zerovalent iron nanoparticles(nZVI) by capping with two different cyclodextrin derived crosslinked polymers CDCA and CDLA obtained from green precursors
2. Assessment of CDCA@nZVI and CDLA@nZVI as catalysts for rapid sonochemical reduction of nitroaromatics in aqueous medium at ambient temperatures
3. Optimization of reaction parameters and a comparison of the performance of the two catalysts.
4. Assessment of recyclability of the catalyst which confirms its stability and robust nature

The catalysts were characterized using NMR, FTIR, EDX, HRTEM, DLS, Zeta potential, FESEM, VSM, XRD, XPS and TGA analysis. 4-Nitrophenol was used as a model substrate and the substrate scope was extended to different nitroaromatic compounds. The products were isolated and characterized with NMR. The recyclable catalysts could be low-cost, eco-friendly and sustainable options for organic transformation in water via sonochemical approach.

2.2 Experimental Section

2.2.1 Materials

Ferric chloride ($FeCl_3$), β- Cyclodextrin (≥ 97% purity) were purchased from Sigma Aldrich and TCI, India respectively. Dimethyl formamide (DMF), Citric acid (CA), Lactic acid (LA), sodium borohydride ($NaBH_4$), 4-Nitroaniline (4-NA), 3-Nitroaniline (3-NA), 2-Nitroaniline (2-NA), 4-Nitrophenol (4-NP), 2-Nitrophenol (2-NP), Nitrobenzene, N, N Dimethyl formamide (DMF) and Dimethyl Sulphoxide (DMSO) were purchased from Spectrochem, India. All the compounds were used as received without further purification. All the solutions were prepared using double-distilled and demineralized water.

2.2.2 Characterization methods

The catalyst preparation was performed using an ultrasonicator of LABMAN make (India), with a tank capacity of 4 L operating at 100 W. ^{1}H and ^{13}C NMR spectra of CDCA and CDLA polymers were recorded on NMR spectrometer (Avance III (400MHz), Bruker, Switzerland) using DMSO-d^6 as the solvent. 2D NMR Spectroscopy i.e, Correlation Spectroscopy (COSY),

Heteroatom Single Quantum Correlation (HSQC) and Nuclear Overhauser Effect Spectroscopy (NOESY) was recorded on NMR spectrometer (Avance Neo (500 MHz), Bruker, Switzerland) using DMSO-d^6 as the solvent. FTIR spectrophotometer (Alpha, Bruker, Switzerland) was used to record FTIR spectra with KBr pellets in range of 4000–400 cm^{-1}. High-Resolution Transmission Electron Microscopy (HR-TEM) was carried out using an electron microscope (Jem-2100F, Jeol, USA) operated at an acceleration voltage of 200 kV. For this purpose, the sample was dried, powered and dispersed in methanol and ultra-sonication was carried out for 30 minutes. Subsequently, that sample was deposited onto a carbon-coated grid at room temperature and it was allowed to air dried, TEM images were then recorded. Energy-dispersive X-ray spectroscopy (EDX) was performed to analyze the elemental composition using JSM-5610 LV, Jeol, USA, instrument in scanning mode attached to FESEM microscope (JSM7600F, Jeol, USA**)**. The analysis was carried out to ensure that the spectrum acquired is a representation of the bulk of the catalyst system. The size distribution of CDCA@nZVI and CDLA@nZVI was analyzed by dynamic light scattering measurements (DLS) recorded on Delso Nano, Beckman Coulter, USA. The zeta potentials were measured with Nano-ZS 90, Malvern Zetasizer, UK. Vibrating sample magnetometer (VSM) analysis was performed using VSM 7410, Lakeshore, Sweden at room temperature. The powder X-ray diffraction (PXRD) patterns were recorded using diffractometer (D8 Discover, Bruker, Switzerland). The X-Rays were generated using a sealed tube and the wavelength of X-ray was 0.154 nm (Cu K-alpha). Samples were prepared by pressing dried powder and patterns were collected with 0.5 step per second and 2θ ranging from 10^o to 90°. The surface compositions and oxidation states were investigated using X-ray Photoelectron Spectroscopy (XPS), performed on ESCA spectrometer **(**SPECS Surface Nano Analysis GmbH, Germany**).** Thermo gravimetric analysis (TGA) was performed using INCARP EXSTAR 6000 (TG–DTA 6300, Seiko, Japan) at a heating rate of 10°C/min in the temperature range of 30–500°C. A nitrogen atmosphere was maintained throughout the measurement. CDCA@nZVI and CDLA@nZVI catalyzed reduction reactions were monitored using UV-Vis Spectrophotometer (Agilent Technologies, Cary 60, U.S) by corresponding λ_{max}.

2.2.3 Synthesis of nanocatalysts derived from cyclodextrin modified polymers capped nZVI

Synthesis of iron nanoparticles was carried out in aqueous solution by reducing ferric ions with

sodium borohydride according to a protocol formulated by Wang and Zhang[33] followed by capping of as prepared nanosized zerovalent iron nanoparticles (nZVI) with two different cyclodextrin derived crosslinked polymers shown in **Scheme 2.1 & 2.2**.

2.2.3.1 Synthesis of citric acid modified cyclodextrin polymer

The crosslinked cyclodextrin citrate ester (CDCA) polymer was synthesized via esterification reaction. Briefly, CD (500 mg, 0.44 mmol) and of CA (100 mg, 0.52 mmol) were dissolved in 10 mL of DMF. To this solution, of DCC (N, N-Dicyclohexylcarbodiimide) (100 mg, 0.48 mmol) acts as coupling agent which in situ activates the carboxyl groups and DMAP (4-Dimethylaminopyridine) (10 mg, 0.08 mmol), acts as a nucleophilic catalyst accelerating the reaction, were added and the reaction was stirred overnight at room temperature (35^{o}C) to assist the ester formation. Upon completion of the reaction after 24 h, the precipitated DCU (1, 3-dicyclohexylurea) was filtered off to obtain the desired product. The polymer was purified by a re-precipitation method using diethyl ether twice. The transparent pale-yellow filtrate was treated with diethyl ether, which gave a white precipitate. The final product was dried under vacuum condition to obtain the stable solid CDCA crosslinked polymer. The final CDCA product (400 mg) was stored at room temperature in dry environment until further use and subsequently characterized.

2.2.3.2 Synthesis of cyclodextrin-citric acid polymer capped Fe nanoparticles (CDCA@nZVI)

To prepare CDCA@nZVI, 10 ml $FeCl_3$ solution (0.1 M) was sonicated for 10 min. Then, 10 ml $NaBH_4$ (0.9 M) solution was added dropwise during the course of 10 min to the $FeCl_3$ solution in an inert condition with nitrogen purging. The reaction mixture was sonicated for next 30 min, to ensure the complete reduction of Fe^{3+} ions to zero valent iron (Fe^0) nanoparticles. To this reaction mixture sodium hydroxide was added dropwise to adjust the pH 8. The resultant solution was sonicated for 10 minutes. Next, CDCA polymer (30mg, dissolved in 5 ml water) was added drop wise and the resultant solution was sonicated for 30 minutes. The reaction mixture was separated by magnetic decantation followed by washing thrice with absolute ethanol. The CDCA@nZVI nanocomposites were then dried in vacuum oven and preserved in vaccuo. Similar procedure was adopted for the synthesis of CDLA@nZVI by using CDLA as the capping agent.

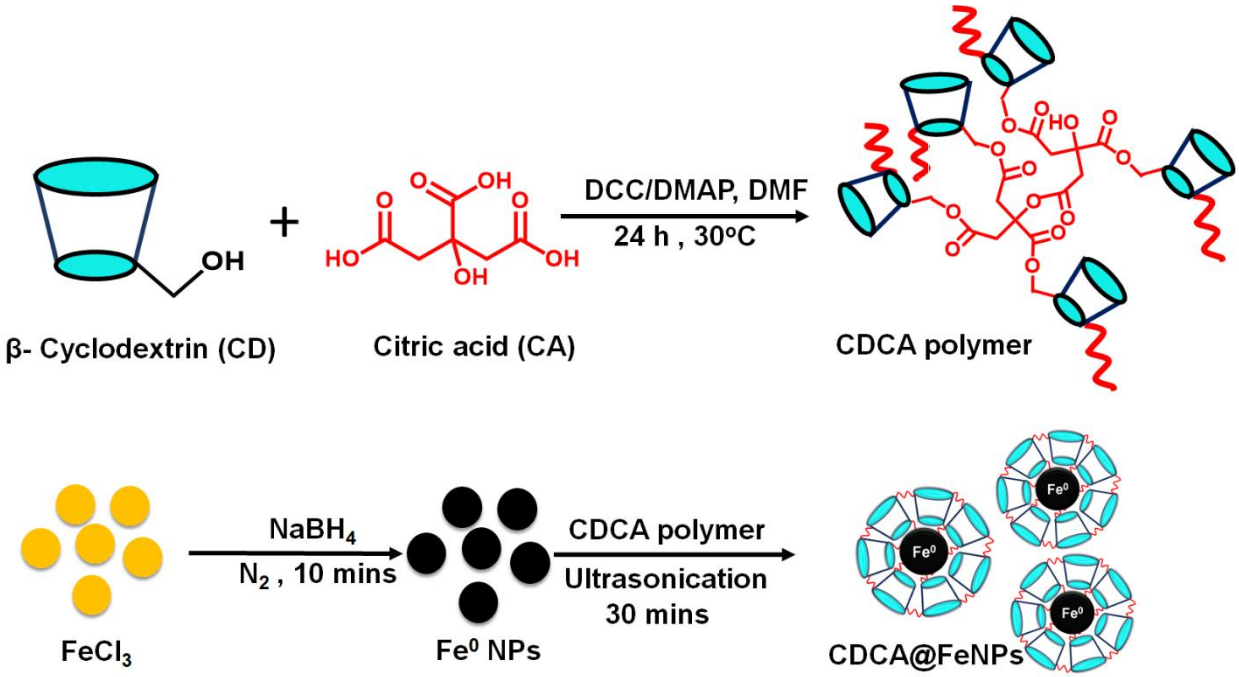

Scheme 2.1: Synthetic route for preparing Citric acid modified β-Cyclodextrin derived polymer capped Fe nanoparticles via ultrasonication method

2.2.3.3 Synthesis of lactic acid modified cyclodextrin polymer

The crosslinked cyclodextrin lactate ester (CDLA) polymer was synthesized via esterification reaction. Briefly, CD (500 mg, 0.44 mmol) and LA (100 mg, 1.11 mmol) were dissolved in 10 mL of DMF. To this solution, DCC (100 mg, 0.48 mmol) and DMAP (10 mg, 0.08 mmol) were added and the reaction was stirred overnight at room temperature (35^{o}C) to assist the ester formation. Upon completion of the reaction after 24 h, the precipitated DCU (1, 3-dicyclohexylurea) was in the solution was filtered off to obtain the desired product. The polymer was purified by a re-precipitation method using diethyl ether twice. The transparent pale-yellow filtrate was treated with diethyl ether, which gave a white precipitate. The final product was dried under vacuum condition to obtain the stable solid CDLA crosslinked polymer. The final CDLA product (430 mg) was stored at room temperature in dry environment until further use and subsequently characterized.

2.2.3.4 Synthesis of cyclodextrin-lactic acid polymer capped Fe nanoparticles (CDLA@nZVI)

To prepare CDLA@nZVI, 10 ml $FeCl_3$ solution (0.1 M) was sonicated for 10 min. Then, 10 ml $NaBH_4$ (0.9 M) solution was added dropwise during the course of 10 min to the $FeCl_3$ solution in an inert condition with nitrogen purging. The reaction mixture was sonicated for next 30 min, to ensure the complete reduction of Fe^{3+} ions to zero valent iron (Fe^0) nanoparticles. To this reaction mixture sodium hydroxide was added dropwise to adjust the pH 8. The resultant solution was sonicated for 10 minutes. Next, CDLA polymer (30 mg, dissolved in 5 ml water) was added drop wise and the resultant solution was sonicated for 30 minutes. The reaction mixture was separated by magnetic decantation followed by washed thrice with absolute ethanol. The obtained product was then dried in vacuum oven and preserved in vaccuo.

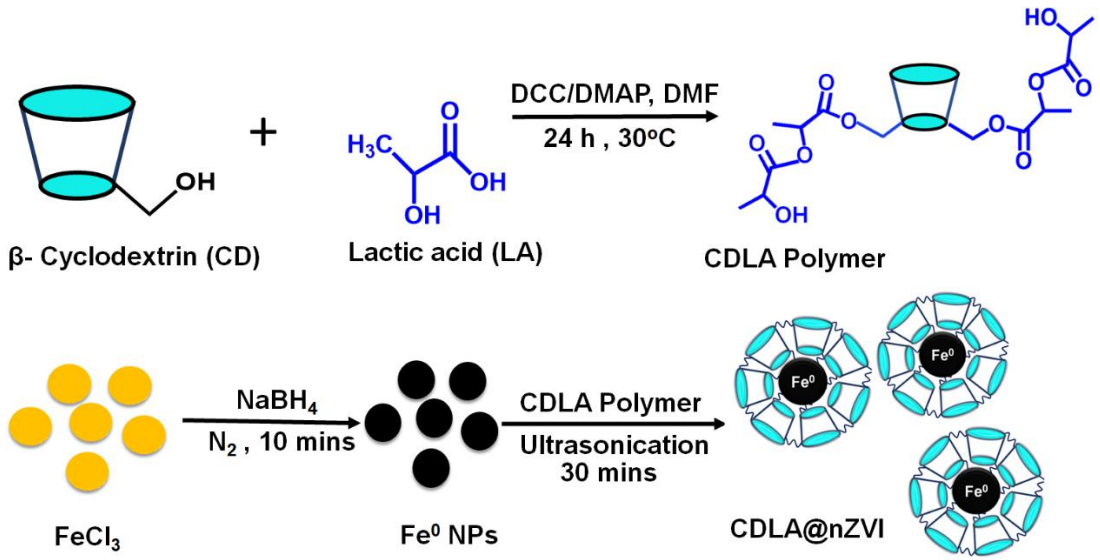

Scheme 2.2: Synthetic route for preparing lactic acid modified β-Cyclodextrin derived polymer capped Fe nanoparticles via ultrasonication method

2.2.4 Catalytic potential of capped zerovalent iron nanoparticles nanocomposites

The reduction of 4-nitrophenol (4-NP) with $NaBH_4$ was used as a model reaction to determine the catalytic activity of synthesized CDCA@nZVI and CDLA@nZVI. In a typical reaction 10 mg of catalyst was added to 1.5 mL 4-NP solution (0.12 mM) under sonication in 10 mL round bottom

flask at 35°C, then freshly prepared 1.5 mL $NaBH_4$ solution (1.8 mM) was added slowly to the above reaction mixture. Initially, a sudden change in colour from faint yellow to intense yellow was observed due to the formation of nitrophenolate ion which finally disappears. The progress of reaction was monitored using a UV-Vis spectrophotometer.

After complete reduction, the catalyst was separated using an external magnet and dried under vacuum after washing with water and ethanol.

2.2.5 Kinetic evaluation of the reduction of 4-NP

The kinetics of CDCA@nZVI and CDLA@nZVI catalyzed reaction was also determined in terms of concentration of 4-NP [1]. It is assumed that no reaction takes place initially due to a time delay. This time delay is defined as an induction period before the commencement of reaction wherein a restructuring of the nanoparticle surface takes place. The restructuring of surface atoms generates catalytically active sites like corners or edges. This helps the initiation of the reaction. It was noted that the pseudo first order reaction kinetics could be employed for the reduction of 4-NP to 4-AP[34]. As the concentration of $NaBH_4$ is far greater than that of 4-NP, the reaction rate is presumably independent of $NaBH_4$ concentration. Hence the rate of the reaction can be evaluated by studying the kinetics of the reaction in terms of the concentration of 4-NP[35]. The rate constant k was determined for the reaction using the plot of ln (C_t/C_0) vs. reduction time as per the following equation (Eq. (1)):

$$\ln\left(\frac{Ct}{Co}\right) = -kt \qquad (1)$$

Where Ct is the concentration of the 4-NP at time t (min), C_0 is the initial concentration of 4-NP at time t = 0 (min) and k is rate constant. The conversion of 4-NP was calculated using the following equation (Eq. (2)):

$$\text{Conversion} = \ln\left(\frac{At}{Ao}\right) X\ 100\% \qquad (2)$$

where At presents the UV absorbance at 405 nm, which is proportional to the concentration of reduced 4-NP; A0 is initial UV absorbance at 405 nm after addition of $NaBH_4$[36].

2.3 Result and Discussion

2.3.1 Synthesis of β-cyclodextrin derived crosslinked polymers for capping nZVI

The synthetic route of the zerovalent iron nanoparticles is illustrated in Scheme 1 & S1. Two cyclodextrin crosslinked polymers synthesized using naturally occurring citric acid and lactic acid and used as capping agents. Both the polymers have several cyclodextrin units of 1135 Da linked together with several citric acid or lactic acid molecules. Hence, the average molecular weight of the polymer would be much above 10,000 Da which makes it insoluble and useful for heterogeneous catalysis. The utilization of a stable capping agent assists in overcoming the aggregation problem associated with nZVI. The citrate/lactate derivative of cyclodextrin polymer with multiple –OH groups are highly stable as result of sonochemical treatment and cannot be removed by solvent washing, thus giving stable polymer capped nZVI nanoparticle. Briefly for the synthesis, solution of ferric chloride in aqueous HCl, was used as a precursor for the zerovalent Fe nanoparticles, obtained by reduction with sodium borohydride under ultrasonication. The polymers capped nZVI were found to be stable and the greyish black colour[24]**.** The rapid catalyst formation occurs as result of cavitation process. This strategy also helps to improve the dispersion of the catalyst which in turn protect and stabilize the incorporated material. The potential of both these catalysts were evaluated for the reduction of various nitroaromatics.

2.3.2 Characterization

The synthesized polymers CDLA and CDCA, as well as CDLA@nZVI and CDCA@nZVI were characterized by various analytical techniques to understand their structure, composition, size, morphology, magnetic and thermal properties as stated below:

2.3.2.1 NMR analysis

The structure of crosslinked CDLA and CDCA polymers was characterized with ^{1}H NMR spectroscopy as shown in **Figure 2.1 & 2.2**. In case of CDLA polymer, the full range ^{1}H NMR spectrum can be simply divided into two zones, the characteristic protons of repetitive β-CD's glucose appear signals at 4.99 ppm (H1), 3.32 ppm (H2), 3.63 ppm (H3), 3.37 ppm (H4), 3.61 ppm (H5), 3.63 ppm (H6), 5.77 ppm (OH-1), 5.61 ppm (OH-2) and 4.50 ppm (OH-6). The peaks in the range of 1.27-1.70 ppm were assigned to the CH_3 protons. The CH proton of lactic acid at 4.3 ppm is overlapped with the protons of cyclodextrin which is difficult to distinguish.

The covalent binding of the lactic acid induced a significant downfield shift for the peaks of the H6' protons bound to the esterified carbon and also to the neighbouring H5' proton of the CD. These peaks, at about 4.2–4.3 ppm (H6') and 3.8 ppm (H5') were assigned by correlating the data obtained from ^{1}H NMR, ^{13}C NMR, DEPT135-NMR and 2D NMR spectroscopy.

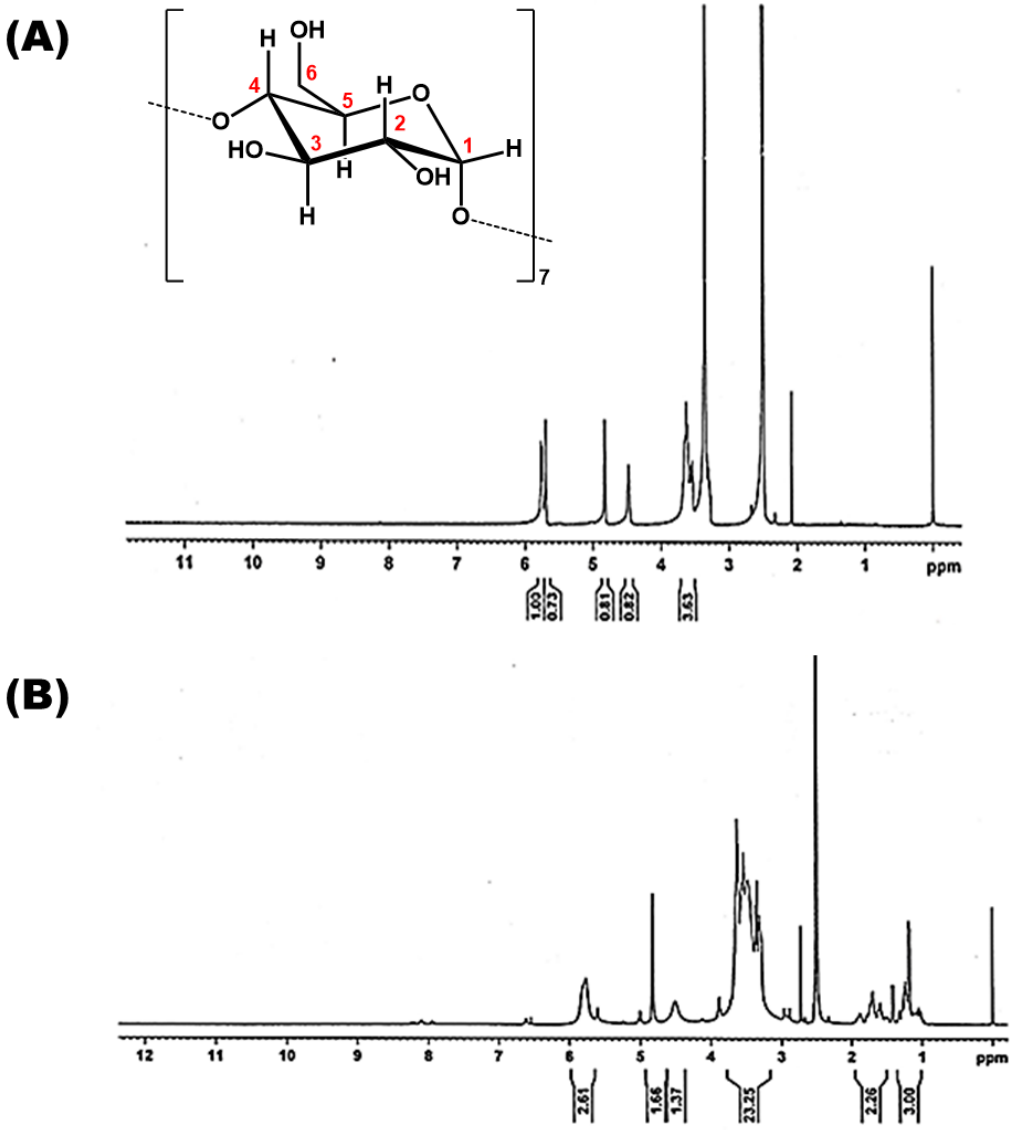

Figure 2.1: ^{1}H NMR of (A) native β-CD and (B) CDLA polymer.

^{13}C NMR spectrum of CDLA polymer showed**,** peak at 101.9 ppm is attributed to C1, peak at 81.5 ppm assigned to C4 and an overlap of C2, C3 and C5 observed at 73.08 ppm, unsubstituted C6 was observed at 59.8 ppm. The substituted C6 of the β-CD is observed downfield at 65.8 ppm. Preferential esterification of β-CD occurs at the primary hydroxy groups as they are sterically less

hindered compared to the secondary hydroxy groups. The appearance of peaks at 21.13 ppm and 65.7 ppm were attributed to the CH_3 and CH of the lactic acid unit, as shown in **Figure 2.2.**

^{1}H-^{1}H COSY (Correlation Spectroscopy) is a suitable technique for determining couplings arising from neighbouring protons. The COSY spectrum (**Figure 2.2**) for CDLA contains both diagonal and cross peaks. The magnetization transfer occurs through bonds to the same type of nucleus (protons) and that make up the cross peaks coordinates. The cross peaks indicate couplings between the two protons, up to three or sometimes four chemical bonds apart. The most apparent cross peak in the spectrum indicates a coupling interaction between methyl protons in the range of 1.2- 1.29 ppm and protons of the β-CD.

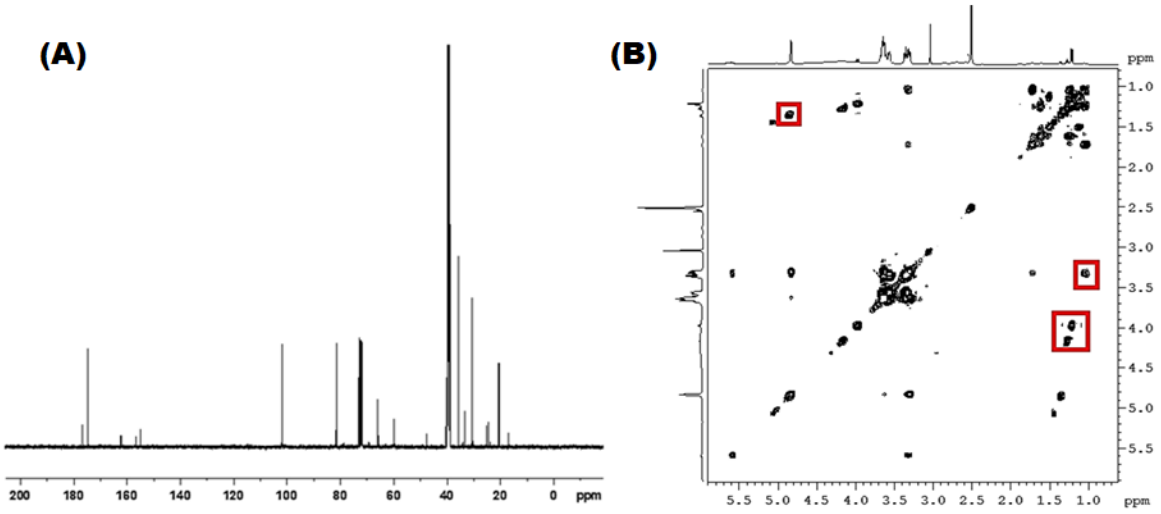

Figure 2.2: (A) ^{13}C NMR and (B) 2D COSY NMR spectrum of CDLA polymer

Figure 2.3 shows the heteronuclear spectra (HSQC) spectra of CDLA polymer and relates the information about ^{1}H and ^{13}C correlations, from which the HSQC spectra shows the correlation peaks of the directly connected ^{1}H and ^{13}C atoms. The methyl proton of lactic acid at 1.23-1.29 ppm correlates with the carbon of methyl at 20.4-16.5 ppm of lactic acid that corresponds to the resonance of the lactic acid methyl carbon signals, as was confirmed by DEPT experiments. In addition to the unsubstituted β-CD C-6 signal at 59.8 ppm, further methylene carbon signals appear downfield in the DEPT spectrum at 64-65 ppm which was assigned to the ester C-6.

NOESY experiments correlate all protons which are close enough to each other. A NOESY spectrum produces through space correlations via spin-lattice relaxation (Nuclear Overhauser

effect, NOE). **Figure 2.3** presents the NOESY spectrum of CDLA having cross-peaks connecting signals from identical nuclei which are spatially close enough. The 2D NOESY-NMR was carried out to investigate the intermolecular interactions between the cyclodextrin and lactic acid in DMSO solution. The space correlation between the magnetically different methylene protons at 4.3 ppm with the methyl proton at 1.29 ppm indicates that the coupled nuclei are close to each other via spatial arrangement in the polymer. The cross-correlation peaks of the methyl protons of lactic acid signals with proton signals of the sugar proton of the cyclodextrin clearly indicates the successful conjugation of lactic acid unit with the cyclodextrin. Evidence for the successful polymerization and intermolecular association obtained from the 2D NOESY NMR spectrum, which indicates correlation peaks between the methyl or methylene signals of lactic acid correspond to the interaction between H-1, H-2 and H-4 of β-CD.

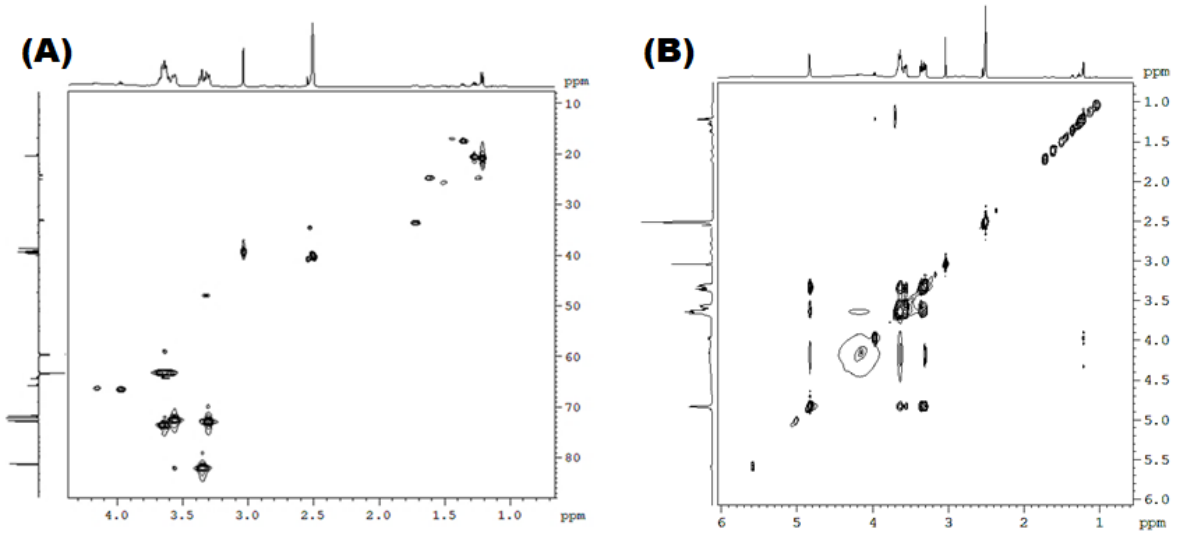

Figure 2.3: (A) 2D HSQC- NMR spectrum and (B) 2D-NOESY NMR of CDLA polymer of CDLA polymer

Similarly, in case of CDCA, the spectra showed the characteristic protons of repetitive β-CD's glucose appear signals at 4.83 ppm (H1), 3.29 ppm (H2), 3.62 ppm (H3), 3.35 ppm (H4), 3.60 ppm(H5), 3.64 ppm (H6), 5.77 ppm (OH-1), 5.71 ppm (OH-2) and 4.51 ppm (OH-6). The -CH_2 protons from the citric acid appeared in the range of 2.5-2.9 ppm, respectively **(Figure 2.4).** This confirms the successful polymer formation.

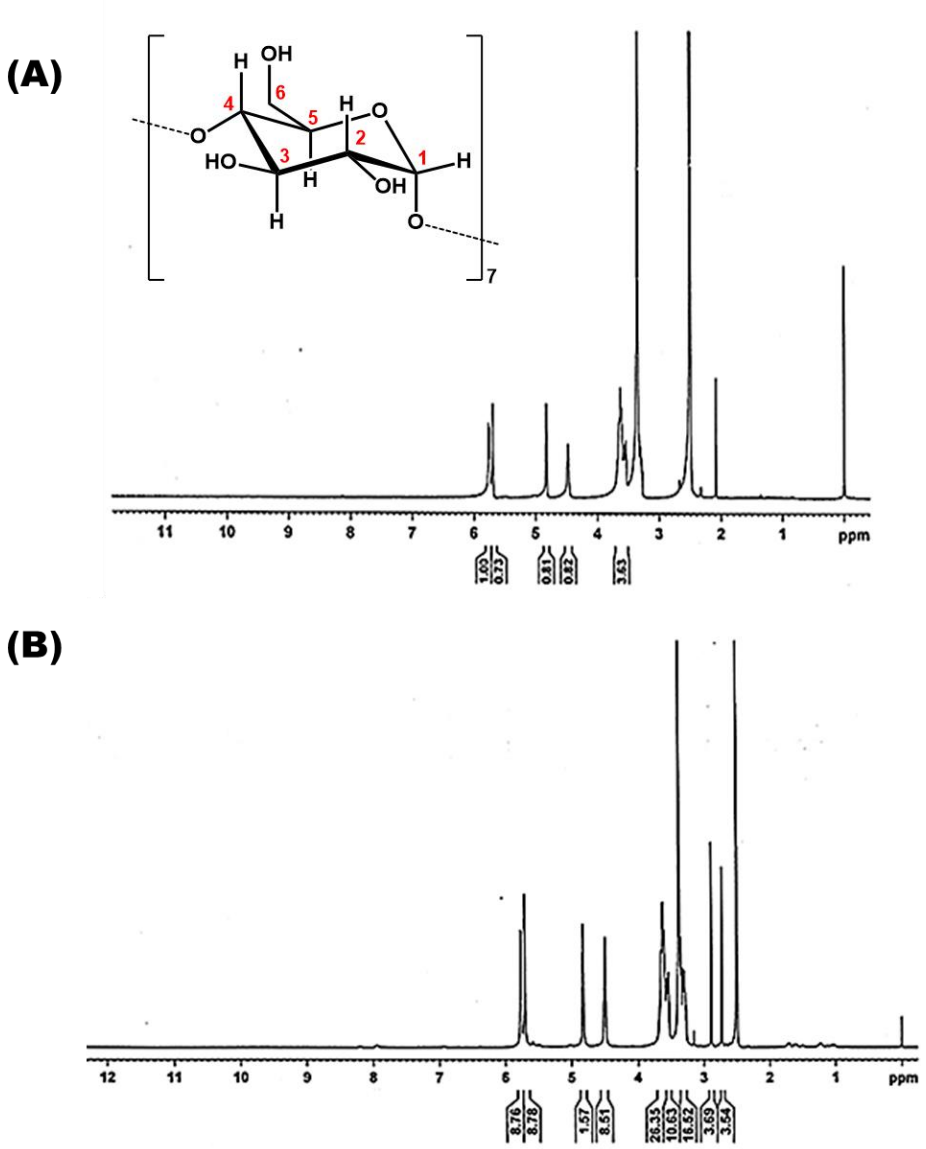

Figure 2.4: **^{1}H NMR of (A) native β-CD (B) CDCA polymer**

Both the β-Cyclodextrin derived crosslinked polymers were also characterized using ^{13}C NMR spectroscopy shown in **Figure 2.5.** Similarly, for CDCA polymer, the carbon from repetitive units of β-CD's glucose units were observed at 102.9 ppm, 81.97 ppm, 72.86 ppm attributed to the C1, C4 and overlap of C2, C3 and C5. The peak at 60.35 ppm was assigned to C6 carbon [37]. The carbon of the citric acid unit in the crosslinked polymer matrix were observed at 43.2 ppm which was attributed to CH_2 of citric acid and the peak observed at 76.9 ppm attributed to the C. The COSY spectrum revealed the cross peaks between the methylene protons and protons of the β-CD. of the CD signal appeared at 65.3 ppm[38].

^{1}H - ^{13}C HSQC NMR of CDCA polymer revealed the methylene protons in the range of 2.5-3.0 ppm correlates with the carbon of methylene at 43 ppm of citric acid. Similarly, the protons correlate with the carbons for β-CD. The unsubstituted C6 of CD was observed at 60.3 ppm and the substituted C6 of the CD signal appeared at 65.3 ppm[38].

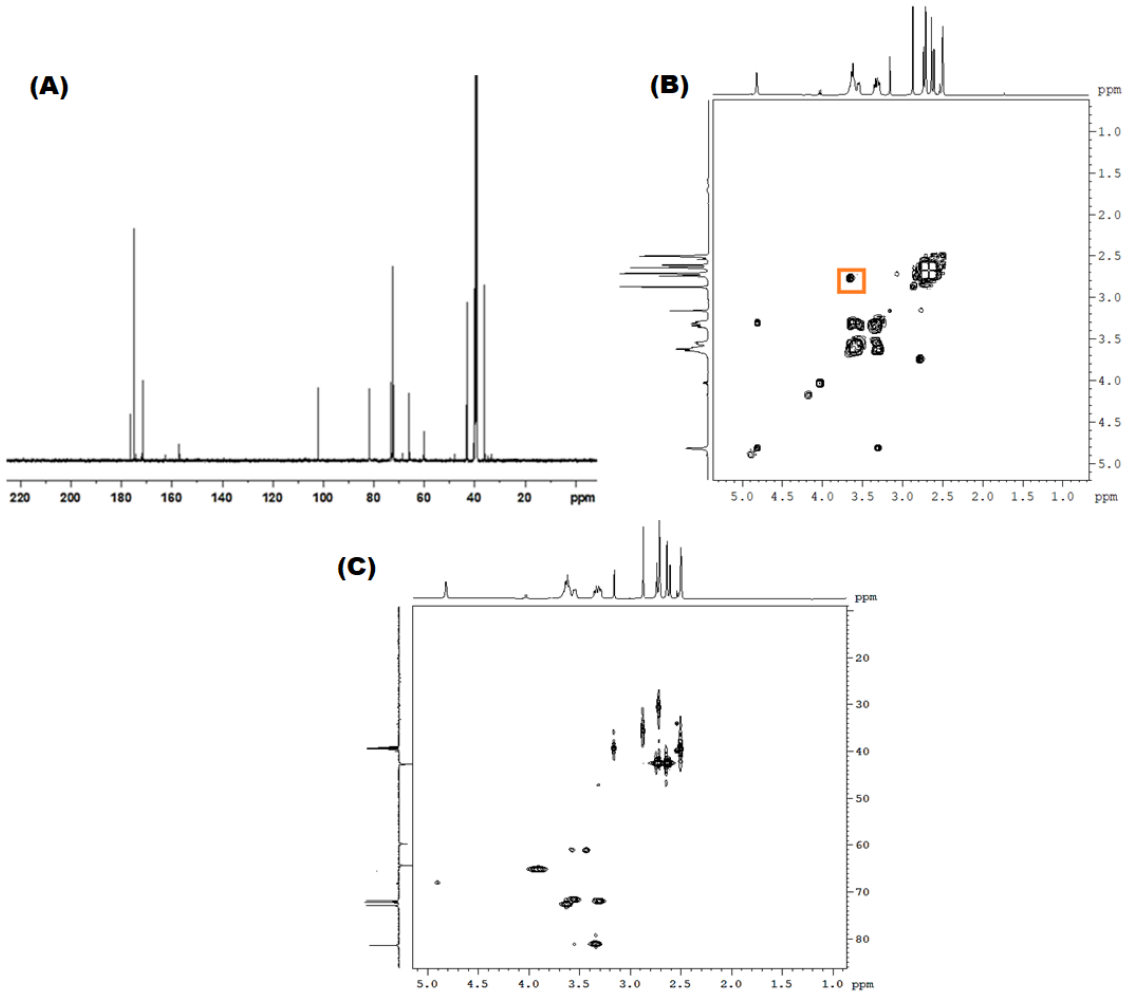

Figure 2.5: (A) ^{13}C NMR and (B) 2D COSY NMR and (C) 2D-HSQC NMR of CDCA polymer

The characteristic peaks for ester linkage formation in case of CDCA appears at 174-176 ppm and for CDLA it was appeared at 171-176 ppm. These results confirmed the successful esterification reaction. The Lactic acid /β-CD molar ratio in the products could then be estimated by integrating the peaks assigned to methyl protons of the lactic acid divided by 7 anomeric protons of β-CD units **(Figure 2.1)**. The degree of substitution (DS) calculated from the ^{1}H NMR data is 3.3. Similarly, for CDCA polymer, by integrating the peaks assigned to methylene protons of the citric

acid divided by 7 anomeric protons of β-CD units. The degree of substitution (DS) was found to be 4.6.

2.3.2.2 FTIR analysis

Citrate modified β-cyclodextrin and lactate modified β-cyclodextrin polymers were formed by the esterification reaction between the hydroxy group (-OH) of β-Cyclodextrin and the carboxyl (–COOH) group of citric acid and lactic acid.

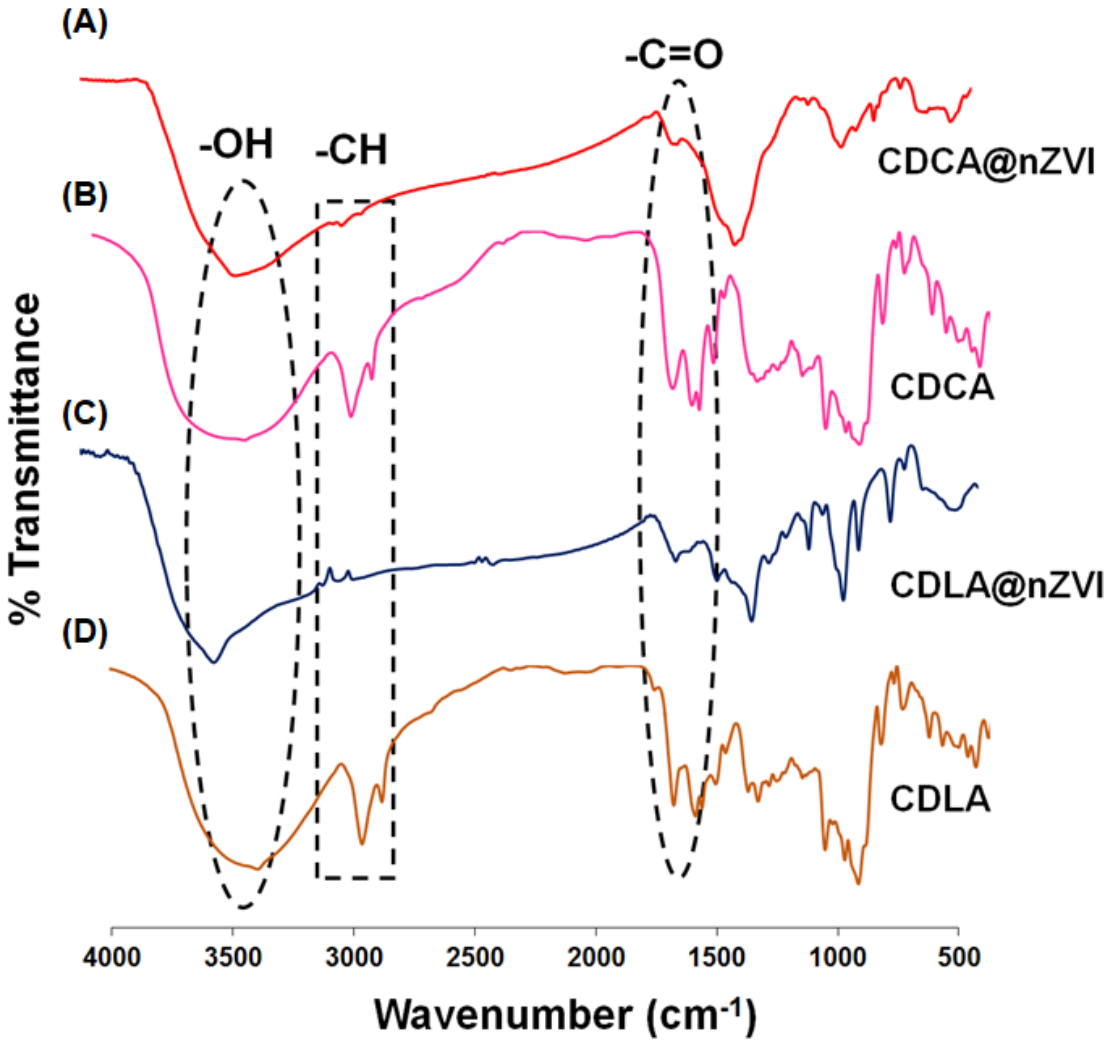

Figure 2.6: Overlay of FTIR spectra (A) CDCA@nZVI (B) CDCA (C) CDLA@nZVI (D) CDLA

Evidence of the polymer formation and successful capping of nZVI were further confirmed by infrared spectroscopy studies as shown in **Figure 2.6**. In case of CDCA polymer, the broad band

was observed at 3329 cm^{-1} which corresponds to the stretching vibrations of OH group. The bands at 2929cm^{-1}, 1155 cm^{-1} and 1029 cm^{-1} corresponds the stretching vibrations of $–CH_2$, –C–O-C-, –C–C and bending vibration of –OH groups, respectively[39]. The band at 1727 cm^{-1} is attributed to the C=O stretching of the ester group, which is a clear indication for the formation of the citrate modified β-CD polymer [39]. Similarly, for CDLA polymer the major broad band at 3320 cm^{-1}, 2929 cm^{-1}, 1155 cm^{-1} and 1028 cm^{-1} correspond to the stretching vibrations of –OH, $–CH_2$, –C–C and bending vibration of –OH groups, respectively. The peak at 1736 cm^{-1} showed the C=O stretching of the ester group, confirms the successful formation of lactate modified β-CD polymer.

Compared with polymer, it was observed that several bands disappeared or shifted and new peaks also appeared corresponding to nZVI. For instance, the absence of C=O peak around 1727cm^{-1} and 1736 cm^{-1} for CDCA and CDLA disappeared indicating the Fe^0 interacted with C=O backbone of the polymer. The peak corresponding to O-H stretching vibration were shifted are observed in the range of 3400-3600 cm^{-1} for polymer and water involved in hydrogen bonding shows the presence of polymer on the surface of nZVI. The peaks observed in the spectra between 900 and 1130 cm^{-1} represented the highly coupled C-C-O, C-OH and C-O-C stretching modes of polymer backbone[24],[40]. From the FTIR analysis, a conclusion could be reached that the surface of nZVI nanoparticles confirms the presence of polymer composition. The obtained results showed that the data is in good agreement with previous findings, which showed that Fe ions interacted with oxygen containing groups in the organic backbone and then converted to inorganic oxides.

2.3.2.3 HR-TEM analysis

The size and morphology of both the catalysts were determined by HRTEM imaging as shown in **Figure 2.7**. HRTEM micrographs confirmed the presence of monodispersed spherical nanoparticles. The mean diameter of both CDCA@nZVI and CDLA@nZVI was found to be in the range of 25-30 nm, with CDCA@nZVI having a size of 30 nm and CDLA@nZVI showed 25 nm. Moreover, a light field contrast was due to polymer coating on the surface of the iron nanoparticles. This also suggests the particles remain uniformly dispersed as both CDCA and CDLA polymers acts as a capping agent wherein the hydroxy groups of the polymer network surround the nZVI and protect the particles over longer periods.

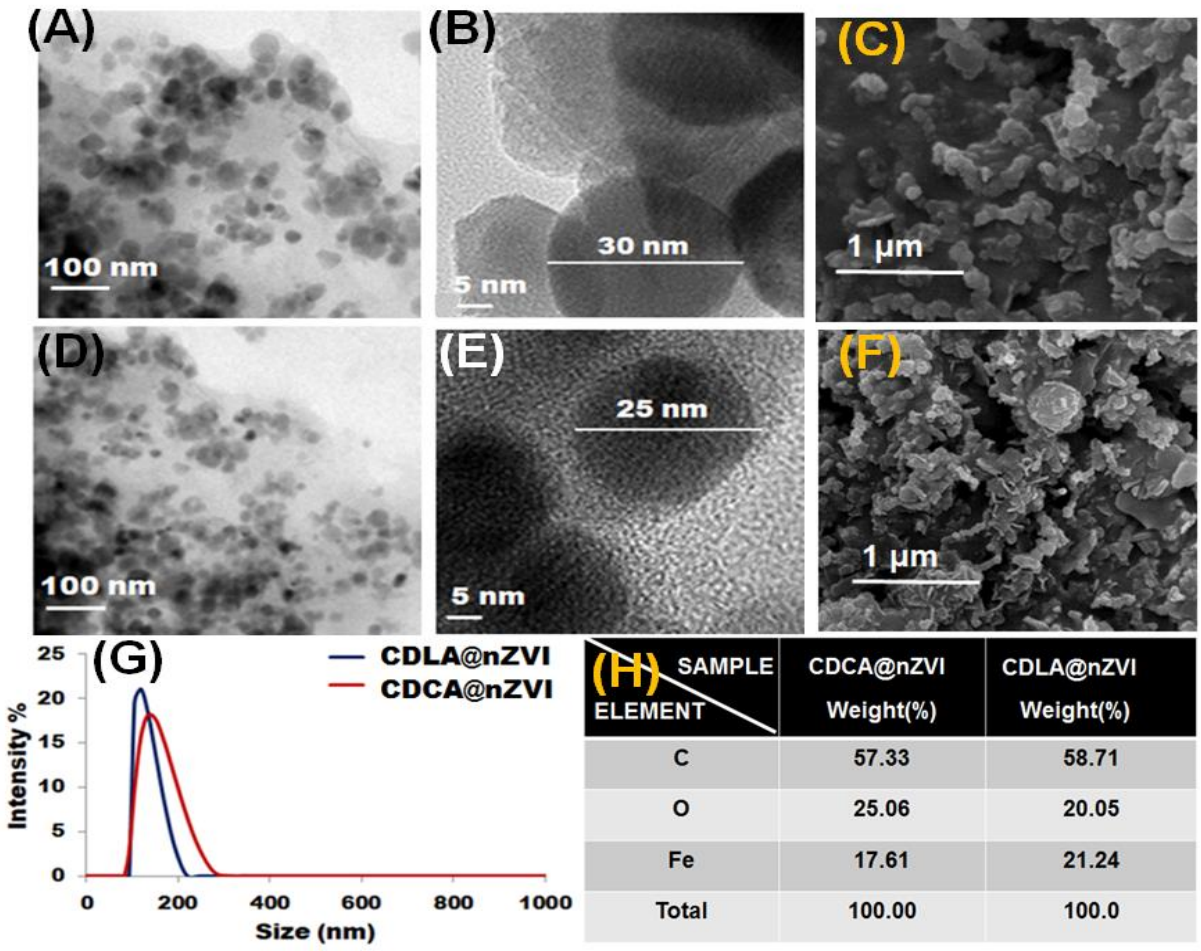

(H)

SAMPLE / ELEMENT	CDCA@nZVI Weight(%)	CDLA@nZVI Weight(%)
C	57.33	58.71
O	25.06	20.05
Fe	17.61	21.24
Total	100.00	100.0

Figure 2.7: Characterization of CDCA@nZVI via (A)HRTEM imaging (B) HRTEM images at higher resolution (C) FESEM micrograph & CDLA@nZVI (D)HRTEM imaging (E) HRTEM images at higher resolution (F) FESEM micrograph showing spherical morphology; comparison of the hydrodynamic size of both catalysts via (G) DLS measurements (H) Elemental composition of both catalysts.

On the other hand, a strong physical adsorption and chemical functionalization of the polymers onto the surface of the nZVI provides better stabilization to the particles formed. The size of nZVI capped with CDLA polymer was found to be smaller as compared to CDCA polymer which leads to the higher surface/volume ratio.

2.3.2.4 Dynamic Light Scattering (DLS)

The hydrodynamic diameters of CDCA@nZVI and CDLA@nZVI were demonstrated using DLS experiments at 25°C (**Figure 2.7 (G)**). The results revealed an average hydrodynamic size of 134

nm for CDCA@nZVI and 118 nm for CDLA@nZVI. Moreover, the particles were monodispersed which is in well agreement with the observations of HR-TEM.

2.3.2.5 Zeta potential analysis

The zeta potential measurements demonstrated -25.23 mV and -29.26 mV charges on the surface of CDCA@nZVI and CDLA@nZVI respectively. The surface negative charge is an attribute of free hydroxy groups on the catalyst surface and values close to -30 mV indicates good stability of the synthesized nanoparticles. The negative zeta potential values help to repel the particles in the suspension resulting in long term stability by avoiding aggregation of the particles.

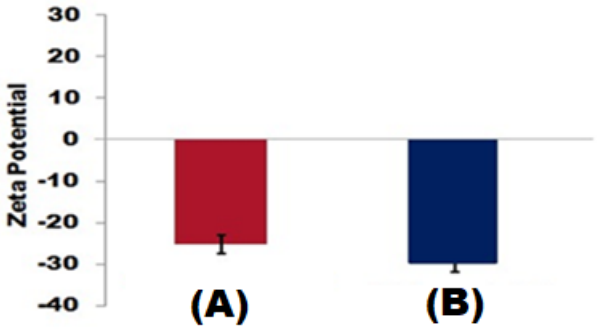

Figure 2.8: Zeta potential measurements (A) CDCA@nZVI and (B) CDLA@nZVI

2.3.2.6 FESEM analysis

The SEM micrographs demonstrated spherical morphology for both the catalysts corroborating with the HRTEM observations (**Figure 2.7(A-C), 2.7 (D-F)**).

2.3.2.7 EDAX analysis

The elemental composition of the both the polymers were obtained by EDX analysis which showed the presence of C and O elements as shown in **Figure 2.9**. The EDX spectra of CDCA@nZVI and CDLA@nZVI are shown in **Figure 2.7(H) & Figure 2.9**. The weight percentage of elemental Fe was found to be 17.61% for CDCA@nZVI and 21.24% for CDLA@nZVI**.** EDX analysis confirms that the final products consist of Fe, O, C elements, due to the absence of any other signals. The presence of elements like C, O and Fe suggest the conjugation of organic functionalities on the surface of the nZVI nanoparticles & successful formation of materials.

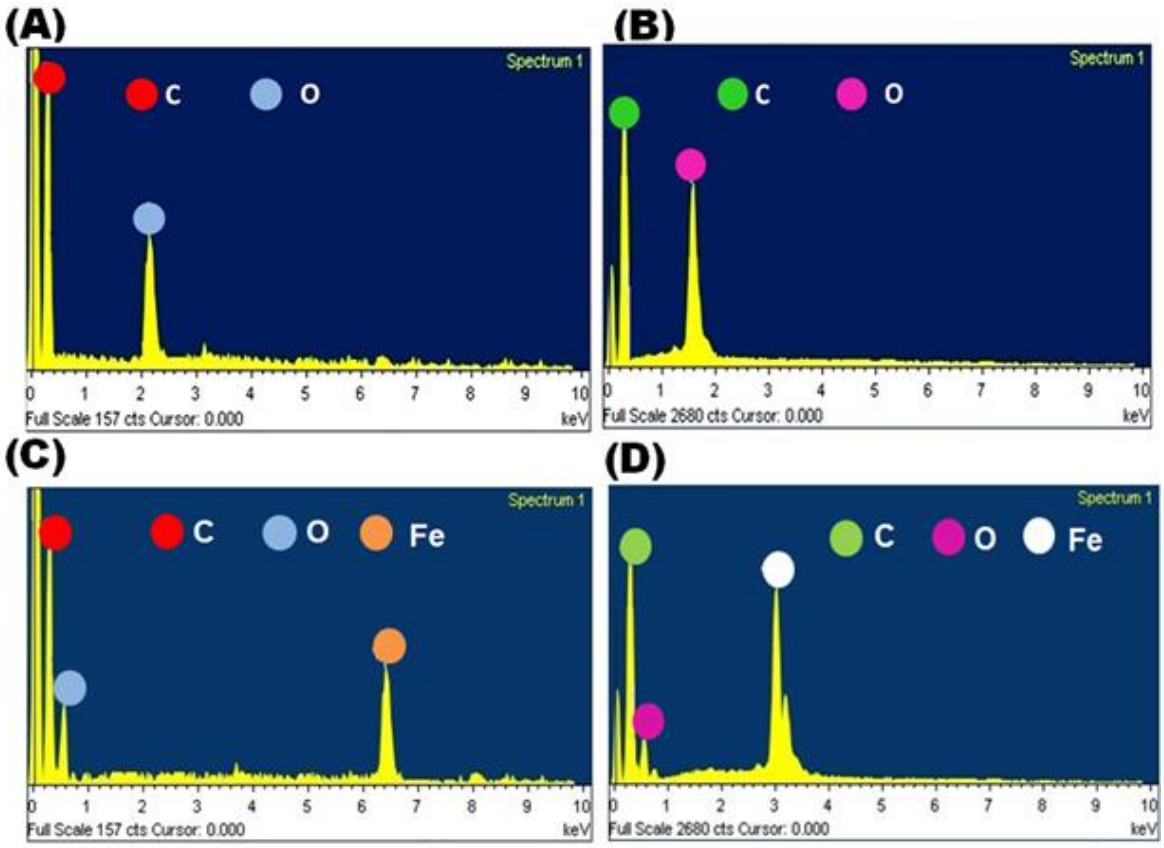

(E)

ELEMENT \ SAMPLE	CDCA Weight(%)	CDLA Weight(%)
C	67.63	69.90
O	32.37	30.10
Total	100.00	100.0

Figure 2.9: Elemental composition as observed by EDAX analysis of (A) CDCA, (B) CDLA, (C) CDCA@nZVI and (D)CDLA@nZVI respectively (E) Elemental composition of CDCA& CDLA polymer.

2.3.2.8 VSM analysis

The evaluation of the magnetic properties of both the catalyst were performed by carrying out vibrating sample magnetometer (VSM) measurements at ambient temperature. The magnetic hysteresis curves of both the catalysts are shown in **Figure 2.10(A) & Figure 2.11(A)**. The

magnetization values were calculated as 22.7 emu g^{-1} and 23.9 emu g^{-1} for CDCA@nZVI and CDLA@nZVI respectively. Thus confirming the superparamagnetic properties of both the catalysts which is also evident from an easy separation using an external magnet[40].

2.3.2.9 XRD analysis

The X-ray diffraction pattern of the as-synthesized CDLA@nZVI and CDCA@nZVI samples are shown in **Figure 2.10(B) & Figure 2.11 (B)**. The broad peak appeared due to the short range order structure discloses the presence of an amorphous phase of Fe (0) nano-phase and it generally occurs due to the surface stabilized iron nanoparticles [24],[41] and it indicates the particles are amorphous in structure.

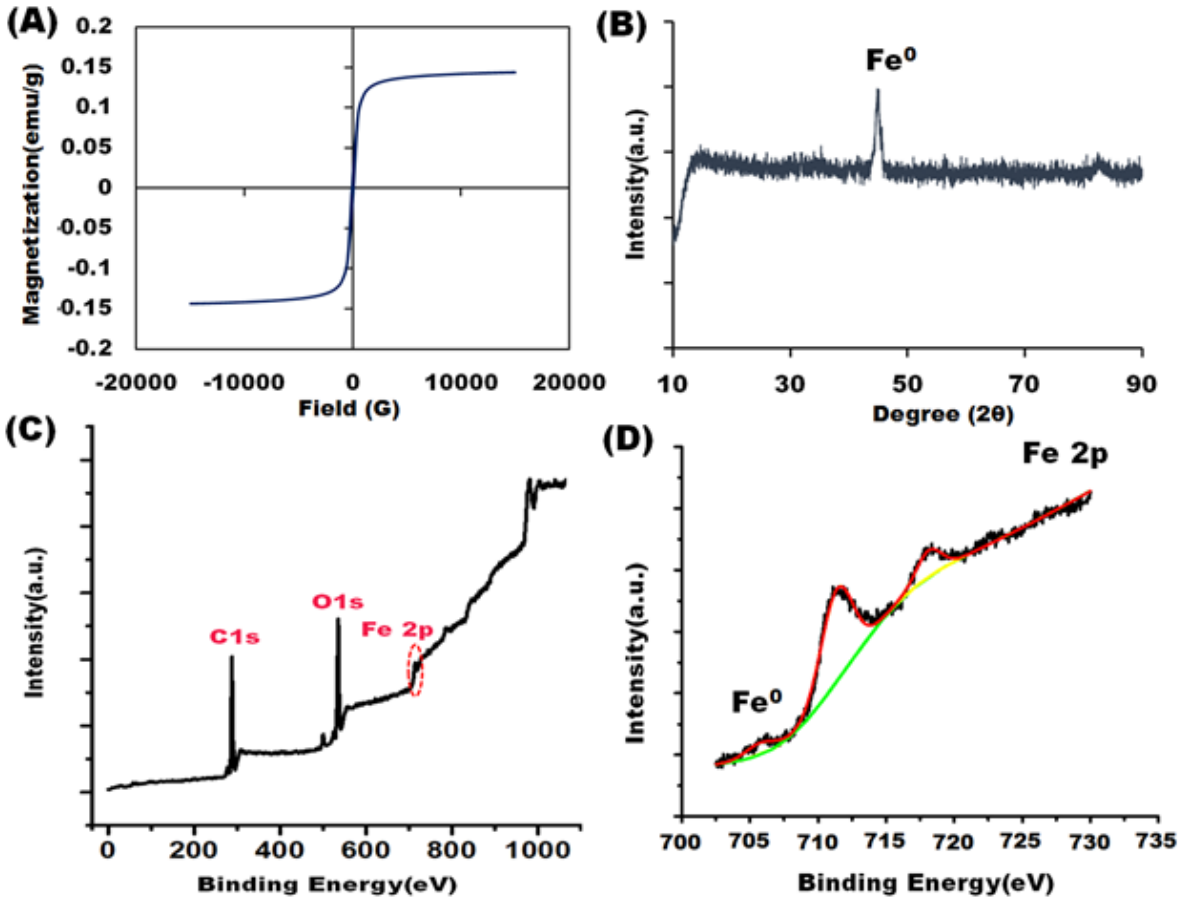

Figure 2.10: Characterization of CDLA@nZVI (A) evaluation of magnetic property via room-temperature magnetization curve (B)XRD spectrum (C) XPS full scan spectrum and (D) graph showing Fe 2p binding state levels as observed in XPS.

XRD demonstrated apparent peaks at 2θ value of 44.9° corresponding to the (110) plane of Fe^0 nanoparticles, indicating the presence of Fe^0 stabilized by CDLA@nZVI and CDCA@nZVI[12],[42].

2.3.2.10 XPS analysis

The XPS spectra for the catalysts successfully provided insights of its surface composition.

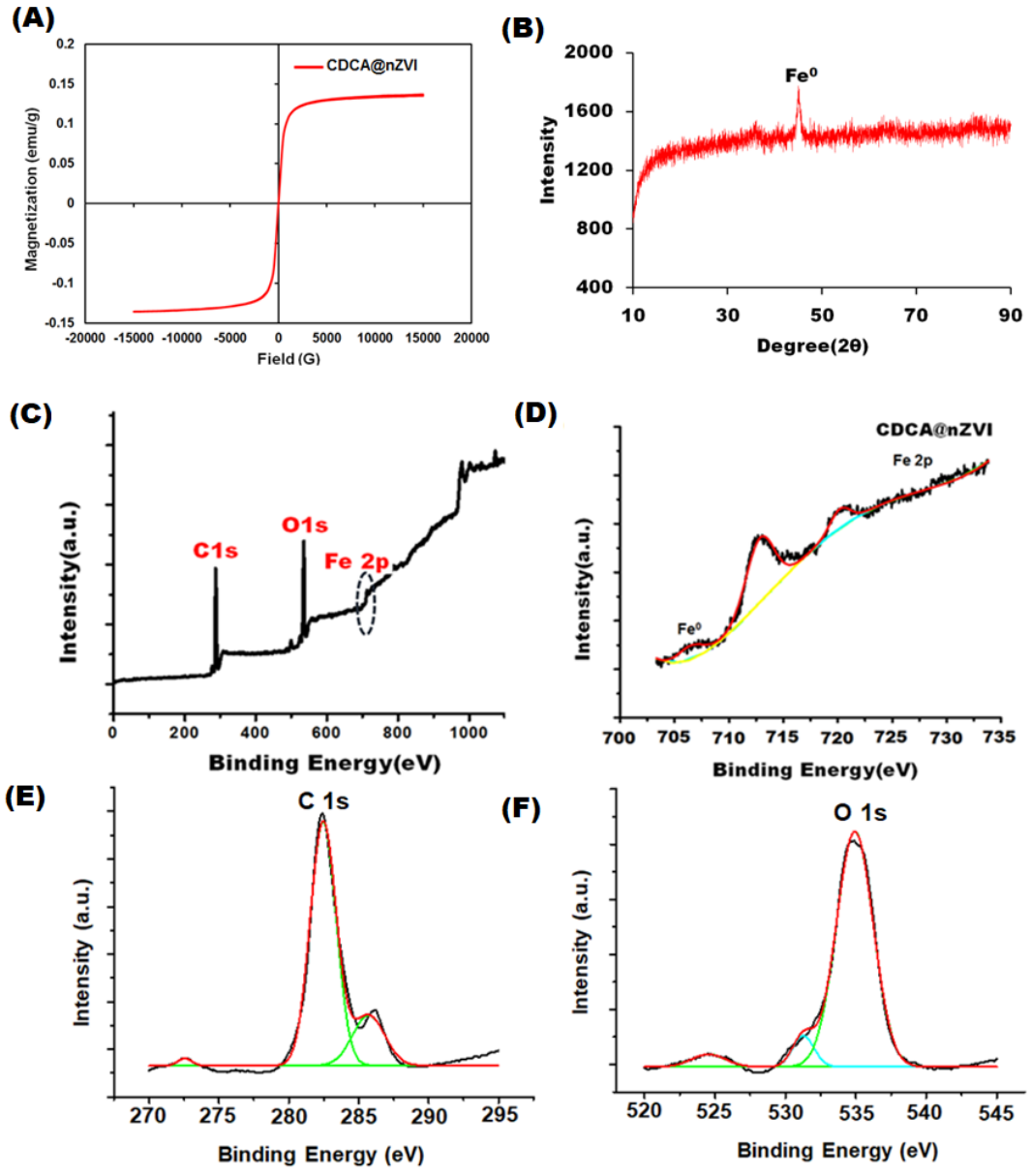

Figure 2.11: (A) Room-temperature magnetization curve, (B) XRD spectrum; XPS spectra (C) Full scan spectrum (D) Fe 2p (E) C 1s and (F) O 1s binding state levels of CDCA@nZVI

A complete scan from 0 to 1000 eV binding energy demonstrated the presence of Fe, C and O elements for both CDLA@nZVI and CDCA@nZVI, corroborating with results of EDX as shown in **Figure 2.10(C)& Figure 2.11 (C-F).**

Since in the XPS analysis the photoelectrons can penetrate only ~5 nm deep from the surface, the Fe^0 peaks observed demonstrate very low intensity and relative area. The Fe^0 peak had much lower intensity compared to the peaks of Fe2p3/2 at 712.5 corresponding to the Fe(III) such as Fe_2O_3& FeOOH and 719.1 corresponding to the overlap of oxidation iron and zero-valent iron[43].

This hindered penetration also confirms the core-shell arrangement of the nanocatalyst with nZVI at the core and the modified cyclodextrin polymer forming the shell. Thus, low binding energies of 706.4 eV and 706.01 eV corresponding to Fe (0) were obtained for CDLA@nZVI and CDCA@nZVI respectively. Thus, the $2p_{3/2}$ peaks of zero-valent iron (Fe) appear as minute shoulder peaks. The obtained XPS results are consistent with the literature reports[34].

The BE corresponding C 1s of C-C linkage was observed at 284.8 eV and at 288.8 eV corresponding to O−C=O linkages[40]. The B.E. for O 1s was observed at 535 eV corresponds to the metallic oxide binding energy[24]. The presence of carbon and oxygen was observed due to the carbohydrate polysaccharide in catalyst composition. It has been reported that an irregular shift in the binding energies O, and Fe is observed as a result of the complex arrangement of atoms within the catalytic framework creating a complex structural environment around these elements. These tend to demonstrate irregular trends in their binding energy values in comparison to that known in literature[44].

2.3.2.11 TGA analysis

The thermogravimetric analysis indicated good thermal stability of both the polymers and the catalysts. The TGA curve of cyclodextrin derived polymer (as shown in **Figure 2.12**) shows mass loss corresponding to 4.73 % occurring in 50-100 °C initially is attributed to the presence of moisture. The next degradation of 12.93% in 100-235 °C was a result of oxidative decomposition of the polymer backbone by the vaporization and elimination of volatile products. The mass loss corresponding to 42.47% upto 400°C occurs due degradation of glycosidic bonds of cyclodextrin in the polymer[24]. The thermogram of CDCA/CDLA capped zerovalent iron nanoparticles showed similar degradation pattern with maximum weight loss of 53% / 45 % upto 500 °C corresponding to the polymeric degradation. The nanocomposite does not undergo a total

decomposition owing to the presence of Fe nanoparticles present in the system.

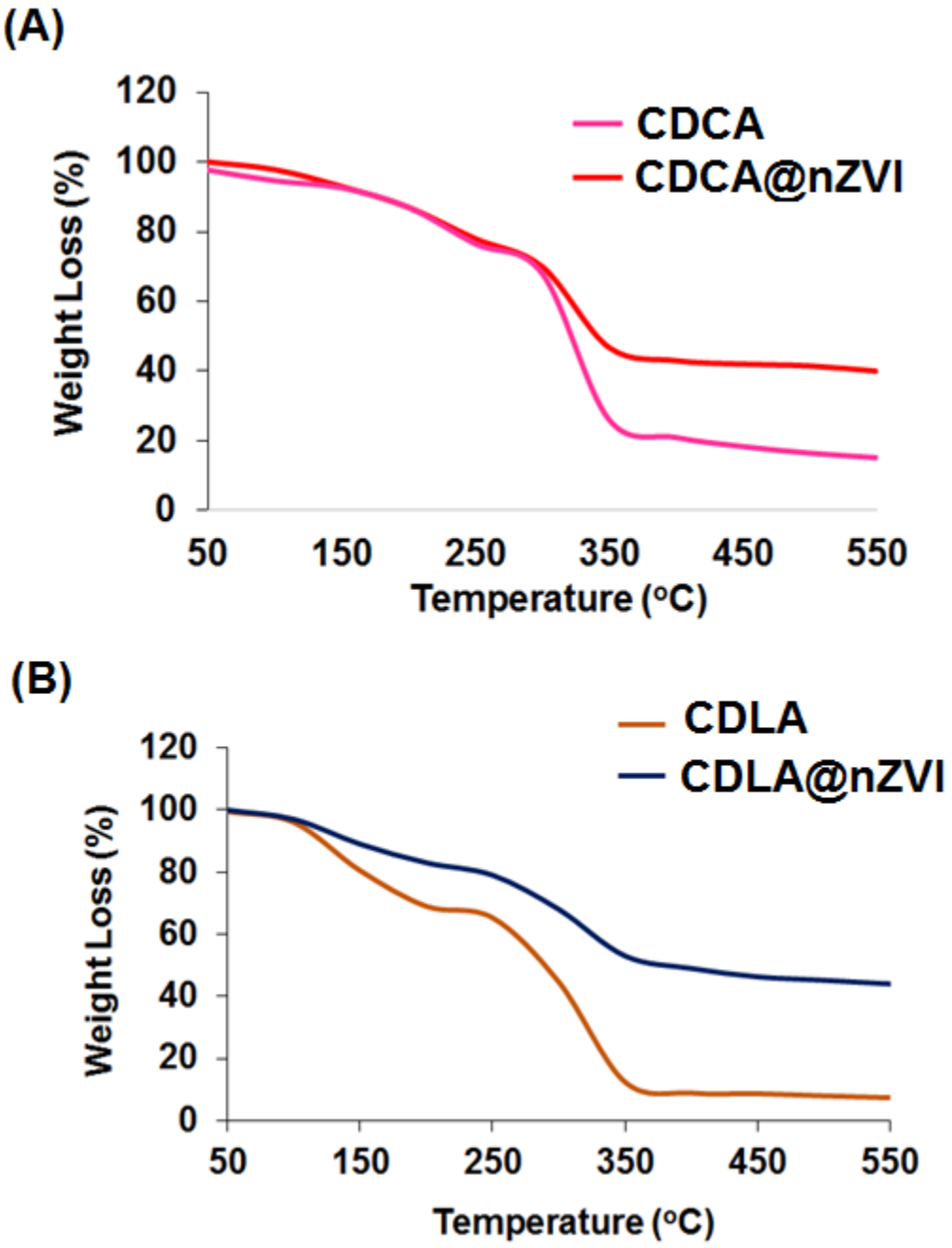

Figure 2.12: TGA curves of (A) CDCA polymer, CDCA@nZVI and (B) CDLA polymer, CDLA@nZVI

2.3.3 Assessment of performance of the catalysts towards reduction of p-nitrophenol

Control experiments were performed with both the catalysts using 4-nitrophenol (0.12 mM) as model reactant and $NaBH_4$ as reducing agent as shown in **Figure 2.13**.

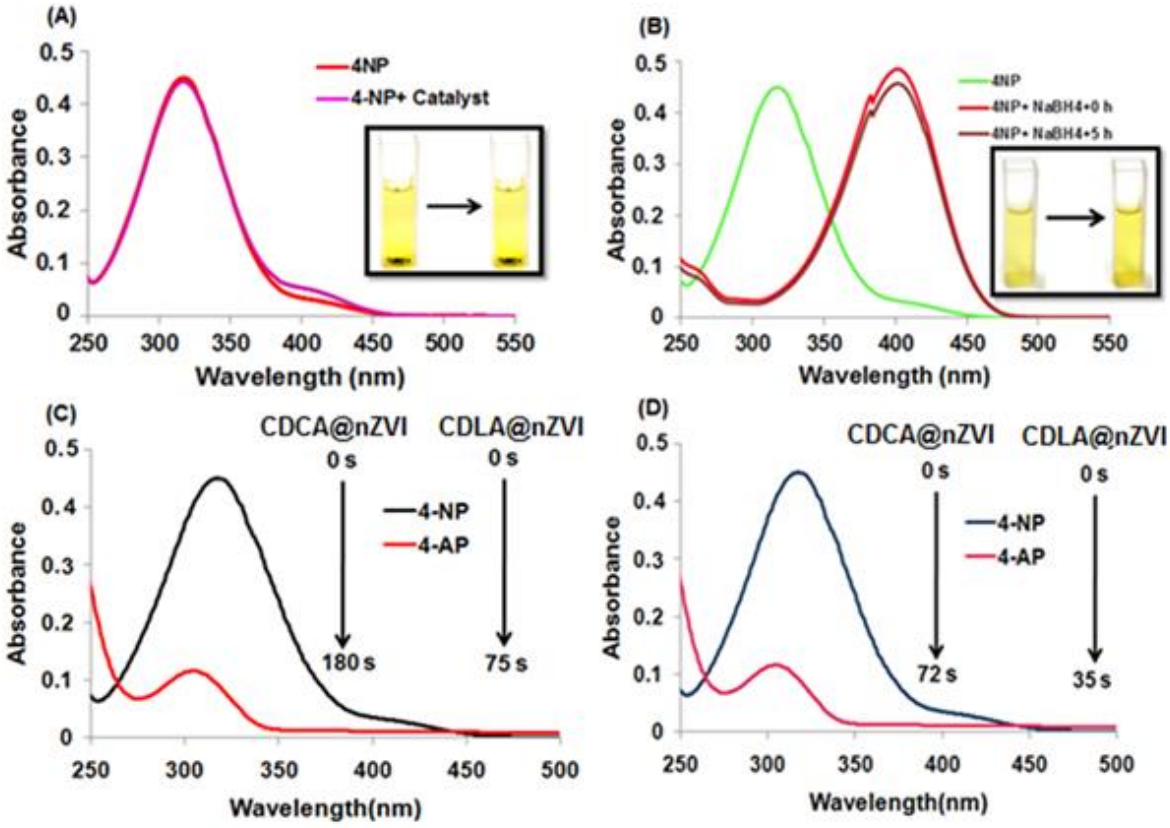

Figure 2.13: UV–Visible absorption spectra of the control reactions performed for the reduction of 4-NP to 4-AP in presence of (A) catalysts only (B) $NaBH_4$ only, (C) in presence of catalysts and $NaBH_4$ (1.8 mM) (D) in presence of catalysts and $NaBH_4$ (2.6 mM).

When both the catalysts and $NaBH_4$ were employed to catalyse the reduction of 4-NP it was observed that the reaction takes place within much lesser time which can be attributed to the fact that iron nanoparticles can help to overcome the kinetic barrier by facilitating electron transfer to the acceptor 4-NP from the donor BH_4^- ions to catalyze the reaction. Reactions were also performed in the presence of only catalyst without adding $NaBH_4$. Under this condition, it was observed that the absorption peak at 317 nm corresponding to the peak of nitrophenol ion remains unaffected indicating that reduction does not take place, as shown in **Figure 2.13 (A).** In another set of control experiments the reduction was attempted only in the presence of $NaBH_4$ without

adding the catalyst. In this case, no change in 4-NP concentration was observed even after 5 h **(Figure 2.13(B))**. These results indicate that presence of both catalyst and $NaBH_4$ is crucial for reduction to take place. This is due to the fact that, inspite of being a thermodynamically favorable reaction, the reduction of 4-NP to 4-AP using only aqueous $NaBH_4$ does not occur as there is a kinetic barrier. Due to this kinetic barrier, there exists a large potential difference between donor (BH_4^-) and acceptor (4-NP) molecules thus it lowering its feasibility. Thus, the roles of both catalyst and reducing agent were established. The detailed experiments were carried out using both the catalyst. The FTIR spectrum of the CDLA catalyst after reaction with 4-NP was recorded (**Figure 2.14**). The redshift of O—H stretching was observed which could be due to the formation of inclusion complex in β-CD cavity (Krawczyk et al. 2021).

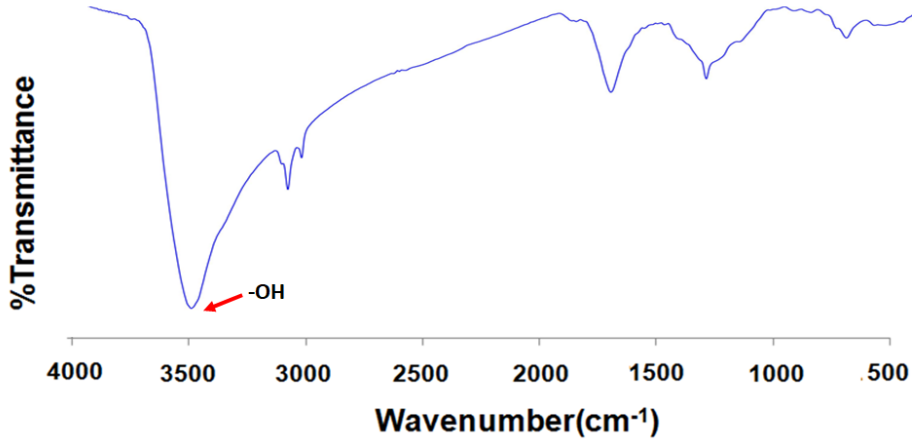

Figure 2.14: FTIR Spectra of CDLA@nZVI after reaction with 4-Nitrophenol

2.3.3.1 Reduction of 4-Nitrophenol using CDLA@nZVI

We investigated the catalytic performance of CDLA@nZVI by selecting the reduction reaction of 4-nitrophenol (4-NP) to 4-aminophenol (4-AP) in the presence of sodium borohydride as probe reaction. The transformation process with the reaction time for the reduction of 4-NP to 4-AP was monitored using UV-visible spectrophotometry. The aqueous 4-NP exhibits the strong absorption peak at 317 nm which was remarkably red shifted to 405 nm after the addition of $NaBH_4$, indicating the formation of nitrophenolate ion intermediate as shown in **Figure 2.13(B).** After the addition of CDLA@nZVI catalyst the absorbance peak intensity at 405 nm decreases gradually with a concomitant increase of new absorption peak at around 300 nm **Figure 2.13 (C) & 2.13 (D)**).

Furthermore, the light-yellow colour of the solution becomes colourless within 75 seconds in presence of $NaBH_4$ (1.8 mM). It was observed when the concentration of $NaBH_4$ was increased to 2.6 mM the time required for completion of reaction was decreased to 35 seconds and the conversion of 4-NP was found to be 99% in the presence of the catalyst (**Figure 2.13 (C), (D)**) which suggests that the 4-NP is almost completely reduced to 4-AP. These results show that the $NaBH_4$ plays a critical role in this catalytic reaction.

2.3.3.2 Reduction of 4-Nitrophenol using CDCA@nZVI

Similar studies were carried out for the CDCA@nZVI catalyst, it was observed that it takes 180 seconds to reduce 4-NP in the presence of $NaBH_4$ (1.8 mM). However, a color change was observed immediately from yellow to colourless in 75 seconds and 97.2% of 4-NP was converted to aminophenol when the concentration of $NaBH_4$ was increased to 2.6 mM **(Figure 2.13 (C), (D)).** The significantly reduced reaction time (less than a minute) can be attributed to the efficient capping of nZVI with the β-CD crosslinked polymers. The recent report with native β-CD capped nZVI catalyst requires 10 minutes to complete the reduction of 4-NP (Krawczyk et. al 2021).

The optimization for reduction reaction was further carried out by varying parameters like catalyst quantity and temperature which are discussed in the following sections.

2.3.3.3 Effect of catalyst amount on reduction of 4-NP

The amount of catalyst was varied in order to determine its effect on reduction of 4-NP as shown in **Table 2.1**. The quantity of catalyst was varied from 3 mg to 15 mg (**Table 2.1; entry 1–5**). When 3 mg catalyst was taken the complete reduction of nitrophenol takes place in 145 s and 120 s on using CDCA@nZVI and CDLA@nZVI catalysts respectively. It was observed that on increasing the amount of catalyst the time taken for the reaction completion decreases, which is due to higher number of active sites. For instance, when catalyst amount was 10 mg the time taken for complete reduction is 75 s and 35 s for CDCA@nZVI and CDLA@nZVI respectively. However, on further increasing the amount to 15 mg, there was no drastic change in reaction time for both the catalysts (**Table 2.1, entry 5)**. Hence 10 mg was selected as the optimum catalyst amount for further experiments.

Table 2.1: Effect of catalyst amount on reduction of 4-NP

Sr. No.	Quantity of catalyst (mg)	Time [a] (s)	Time [b] (s)
1.	3	145	120
2.	5	120	106
3.	7	84	66
4.	10	75	35
5.	15	72	34

Reaction conditions: 1.5 mL 4-NP (0.12 mM), 1.5 mL $NaBH_4$ (2.16 mM), room temperature (35°C), Catalyst ([a] CDCA@nZVI and [b] CDLA@nZVI).

2.3.3.4 Effect of temperature in the reduction of 4-NP

The effect of temperature on the activity of both the catalyst were also assessed. For the study, the reaction was performed at three different temperatures viz. 35°C, 45°C, and 55°C and reaction times are mentioned in **Table 2.2.** There was a drastic decrease in reaction time upon increasing the reaction temperature from 35 to 55°C **(Table 2.2, entry 1-3)**. This decrease is attributed to increased diffusion rate of reactants towards Fe nanoparticles at higher temperatures.

Table 2.2: Effect of temperature in the reduction of 4-NP

Sr. No.	Temperature	Time [a] (s)	Time [b] (s)
1.	35°C	75	35
2.	45°C	60	23
3.	55°C	55	10

Reaction conditions: 1.5 mL 4-NP (0.12 mM), 1.5 mL $NaBH_4$ (2.16 mM), 10 mg catalyst ([a] CDCA@nZVI and [b] CDLA@nZVI).

2.3.4 The reaction kinetics for the catalytic reduction of p-nitrophenol

The reaction kinetics for the catalytic reduction of p-nitrophenol to p-aminophenol was performed at 35°C, and the progress of the reaction with time was determined by UV-vis spectroscopy displayed in **Figure 2.15**. To estimate the reaction rate constants k, the pseudo-first order rate kinetic model was employed at different time intervals[34],[1]. The plot of ln (Ct/C0) (C is the absorbance at 405 nm) vs. reduction time (t) showed a linear relationship for both catalysts.

As the concentration of $NaBH_4$ is much higher than that of 4-NP, the reaction rate is independent of $NaBH_4$ concentration.

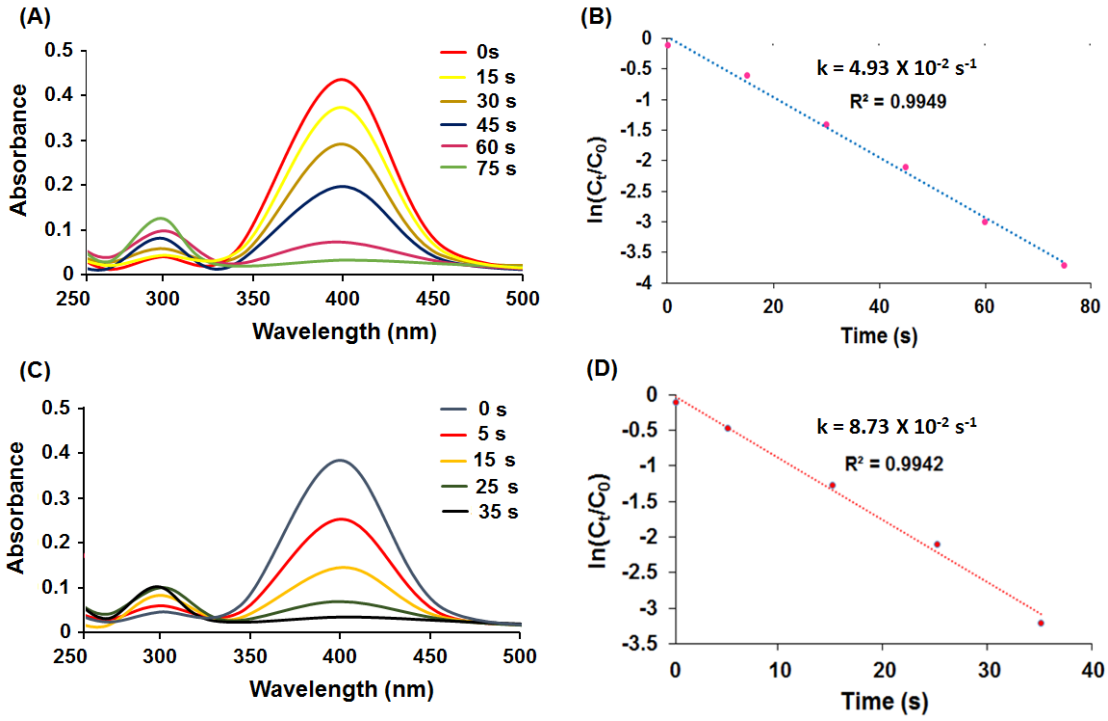

Figure 2.15: The time dependent UV-vis absorption spectra of 4-NP reduction and the dependence of ln(C/Co) versus time plot for the pseudo-first-order reaction kinetics in the presence of (A, B) CDCA@nZVI and (C, D) CDLA@nZVI at 35°C.

The correlation coefficient obtained was 0.9949 and 0.9942 when CDCA@nZVI and CDLA@nZVI were used as catalyst, respectively thus ensuring good linearity. The values of rate constant k obtained from modelling was $4.93X10^{-2}$ s^{-1} for CDCA@nZVI and $8.73X10^{-2}$ s^{-1} for CDLA@nZVI **(Figure 2.15(B) and** 2.15**(D))**, which is higher than various other catalysts summarized in **Table 2.3.**

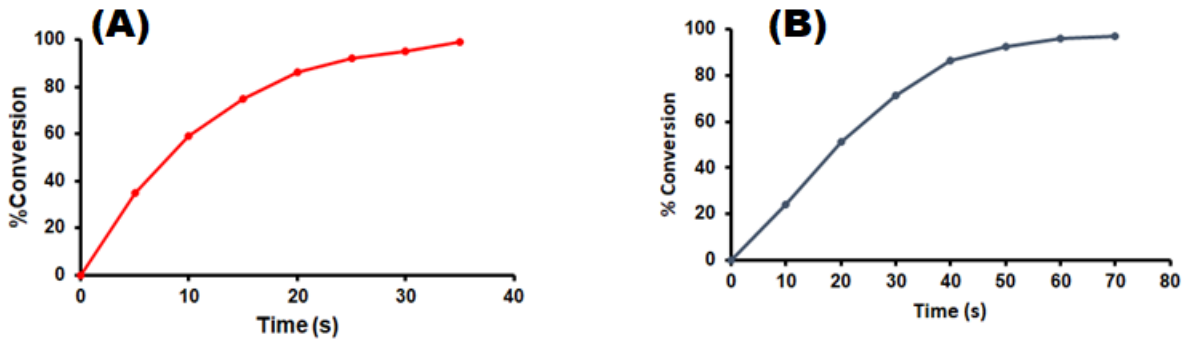

Figure 2.16: Plot of % conversion of 4-NP (A) CDLA@nZVI (B) CDCA@nZVI.

Table 2.3: Comparison of 4-NP reduction in the presence of $NaBH_4$ as a reducing agent with various catalysts.

Sr. No	Catalysts	Concentration of Catalyst	k	Reference
1	nZVI@C-Au-1	4 mg	0.28 min^{-1}	[17]
2	AgNC	10 mg	0.6787 min^{-1}	[1]
3	Bentonite clay supported Fe NPs	10 mg	0.1409 min^{-1}	[7]
4	Au@CPF-1	20 mg	5.05X 10^{-3} s^{-1}	[45]
5	Hg/Pd NPs	1.6 mg	58.4 X 10^{-3} $\mathbf{s^{-1}}$	[46]
6	Ultra-small ZVI nanoclusters	0.44mM	0.0683 $\mathbf{s^{-1}}$	[34]
7	Fe3O4/Pd@C	5 mg	3.26×10^{-3} s-1	[47]
8	Pd/Fe_3O_4@ γ-Al00H-YSMs	0.05 mg	0.37 X 10^{-3} $\mathbf{s^{-1}}$	[48]
9	**CDCA@nZVI**	**10 mg**	**4.93X10^{-2} s^{-1}**	**This study**
10	**CDLA@nZVI**	**10 mg**	**8.73X10^{-2} s^{-1}**	**This study**

These results thus established that utilization of lactate modified cyclodextrin polymer as a stabilizing agent for capping nZVI caused two-fold enhancement in the catalytic activity as compared to the case when citrate modified cyclodextrin polymer was used. Moreover, the

physical effects of the sonication in an aqueous medium include effective mass transfer through turbulent mixing and acoustic streaming which increases the rate of reaction.

Table 2.3 shows a comparison of rate constants determined from kinetic study. It is seen that the values of the rate constants for both the catalysts are of the same order as other Fe catalysts and also some precious metal catalysts.

2.3.5 Catalytic reduction of various nitroaromatics

It has been proved from above experiments both the catalytic systems have good catalytic activity for 4-NP. Experiments were carried out to evaluate the capability of CDCA@nZVI and CDLA@nZVI to reduce other nitro aromatic compounds. We have investigated the scope of converting various nitroaromatics to respective nitroamines using catalysts, $NaBH_4$ and water under optimized reaction conditions.

Table 2.4 represents the reduction of various nitroaromatics to respective amines using CDLA@nZVI and CDCA@nZVI**.** UV-vis spectra of all the substrates are shown in **Figure 2.17.**

On comparing all the substrates, it was observed that the 2-Nitrophenol showed higher reactivity and takes lesser time compared to 4-Nitrophenol (**Table 2.4, entry 1**). It is well reported in the literature, that the reaction proceeds through the nitrophenolate ion, which is stabilized by resonance due to the presence of an electron-withdrawing nitro group. 4-NP is more stable than 2-Nitrophenol due to steric effect as it takes more time to reduce (**Table 2.4; entry 2)**.

Among nitroanilines, the reduction of 3-nitroaniline is the fastest and takes lesser time than 4-nitroaniline. 2-nitroaniline and 4-nitroanilne are resonance stabilized which makes them stable towards the reaction. Upon comparison, 2-ntroaniline and 4-Nitroaniline, 2-Nitroaniline is less stable than the latter due to steric effects as it takes lesser time to reduce (**Table 2.4; entry 3**).

On the other hand, 3-nitroaniline, having an amine group at meta position is resonance destabilized and hence reacts very fast as compared to the other two nitroaniline. Among 4-Nitroaniline has the most stable anion in the alkaline medium, thereby making it least reactive and takes longer time for reduction to occur (**Table 2.4; entry 4**).

Table 2.4: Reduction of some nitro aromatic compounds to corresponding aromatic amines using CDLA@nZVI at optimized conditions

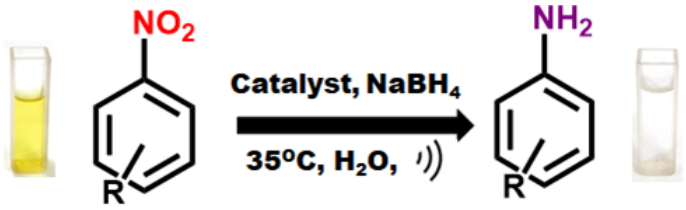

Sr. No.	Substrate	Product	Time [a] (s)	Time [b] (s)
1.	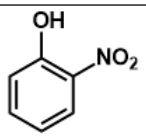	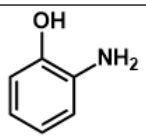	50	165
2.	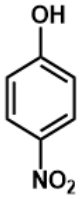		70	210
3.	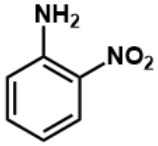	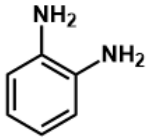	35	89
4.	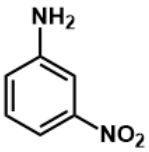	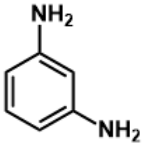	14	50
5.	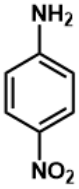	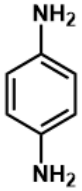	61	114
6.	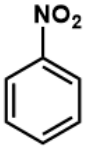	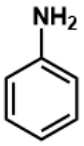	35	100

Reaction conditions: All reactions carried out at room temperature (35°C),1.5 mL of substrate (0.24 mM), catalyst 10 mg (CDLA@nZVI[a], CDCA@nZVI[b]), 1.5 mL $NaBH_4$ (2.16 mM).

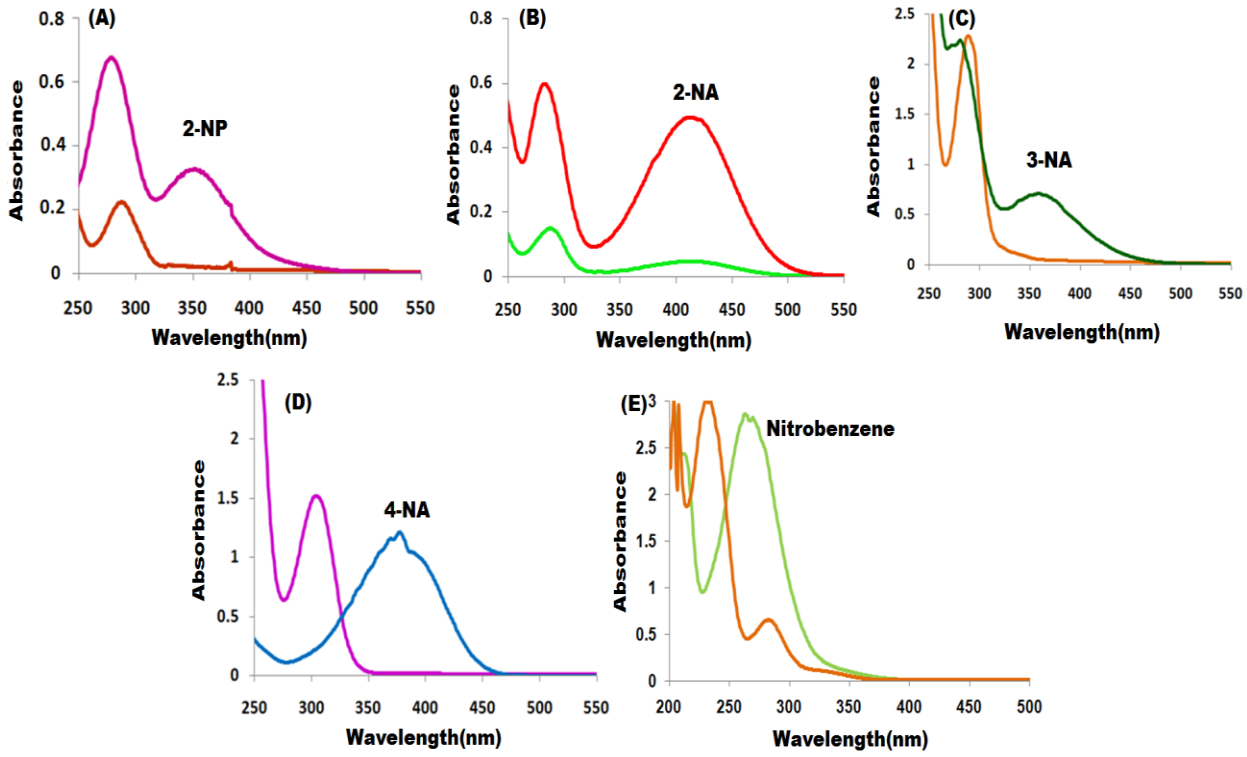

Figure 2.17: UV-visible spectra showing conversion of (A) 2-Nitrophenol (B) 2-Nitroaniline (C) 3-Nitroaniline (D) 4-Nitroaniline (E) Nitrobenzene to respective amines

As the nitrobenzene is less soluble in water, a water-ethanol (95:5, v/v) solution was used as solvent (**Table 2.4; entry 5**). We observed that the nitrobenzene has the least stability and highest reactivity, which is evident from the very small reduction time required, as is evident from the absorption spectra. Similar trends were observed for both the catalyst. And it was observed that the lactic acid derived catalyst takes lesser time.

2.3.6 Scale up experiments

The catalytic reduction was conveniently performed in simple laboratory set up and monitored using UV-vis spectrophotometry. To testify the product formed after the reduction of nitroarene in the presence of $NaBH_4$ and catalyst, the reactions were carried out as follows:

4-Nitrophenol (0.6 mmol), catalyst (25 mg), $NaBH_4$ (9 mM) and water (10 ml) were added in the round bottom flask. The mixture was sonicated, and after the reaction completion the catalyst was magnetically separated. The product was extracted in dichloromethane and solvent was evaporated. The crude product was further purified using column chromatography (0-30% ethyl

acetate in hexane v/v). The product isolated after the reduction of 4-nitrophenol in presence of catalyst and $NaBH_4$ has been confirmed to be 4-aminophenol by NMR spectroscopy (**Spectra data Figure S1).**

Table 2.5: Reduction of some nitro aromatic compounds to corresponding aromatic amines using CDLA@nZVI with isolated yield and TOF.

Sr.No.	Substrate	Product	Time (min, ±2)	Yield [a] (%, ±2)	TOF (min^{-1})
1.	2-Nitrophenol	2-aminophenol	5	91	3.15
2.	4-Nitrophenol	4-Aminophenol	7	92	2.25
3.	2-Nitroaniline	o-Phenylenediamine	4	95	3.94
4.	3-Nitroaniline	m-Phenylenediamine	2	92	7.89
5.	4-Nitroaniline	p-Phenylenediamine	9	91	1.75
6.	Nitrobenzene	Aniline	6	90	2.63

Reaction conditions: All reactions carried out at room temperature (35°C), substrate (0.6 mM), CDLA@nZVI catalyst (25 mg), $NaBH_4$ (9 mM), water (10 mL)., [a] Isolated yield after column chromatography, TOF was calculated on the basis of nZVI nanoparticles.

From the NMR spectra, it can be observed that the OH group appeared at 8.32 ppm, NH_2 appeared at 4.38 ppm and the 4 aromatic hydrogens appeared in the range 6.49-6.41 ppm, thus confirming the solitary product to be aminophenol.

Reduction, isolation and purification of the other nitroaromatics, was carried out in a similar manner. The NMR spectra of the reduction products establish the structure of the corresponding amines (**Figure S2-S6**). To evaluate the catalytic activity of a catalyst, one of the important factors is the Turn over Frequency (TOF). TOF for both the catalysts was calculated by dividing Number of moles of 4-NP that has reacted by Number of moles of nZVI nanoparticle in the catalyst per reaction time. All the nitro substrates were reduced in good yield with both the catalysts. When CDLA@nZVI was used as catalyst, the turnover frequency (TOF) was found to be in the range of 2 to 8 per site min and for CDLA@nZVI it was found to be in the range of 1 to 2 site per min

(**Table 2.5 & 2.6**). It can be concluded from the results that the CDLA@nZVI has better catalytic performance compared to CDCA@nZVI.

Table 2.6: Reduction of some nitroarenes to corresponding aromatic amines using CDCA@nZVI at optimized conditions with isolated yield and TOF.

Sr. No.	Substrate	Product	Time (min, ±2)	Yield [a] (%, ±2)	TOF (min^{-1})
1.	2-Nitrophenol	2-Aminophenol	10	90	1.90
2.	4-Nitrophenol	4-Aminophenol	15	91	1.26
3.	2-Nitroaniline	o-Phenylenediamine	12	94	1.58
4.	3-Nitroaniline	m-Phenylenediamine	8	92	2.38
5.	4-Nitroaniline	p-Phenylenediamine	14	91	1.36
6.	Nitrobenzene	Aniline	11	89	1.76

Reaction conditions: All reactions carried out at room temperature (35°C), substrate (0.6 mM), CDLA@nZVI catalyst (50 mg), $NaBH_4$ (9 mM), water (15 mL), [a] Isolated yield after column chromatography, TOF was calculated on the basis of nZVI nanoparticles.

2.3.7 Recycling and Regeneration studies

Considering the practical applicability of CDCA@nZVI and CDLA@nZVI for the reduction reaction, it is important to assess the recyclability and regeneration of the catalyst. Both the catalysts were recovered easily from the reaction medium using an external magnet due to their inherent magnetism. It was retrieved after each run and washed with water followed by ethanol to ensure removal of unwanted remnants from the surface and dried at 60°C in vacuum oven. Then the dried catalysts were treated with a new round of reduction reaction to investigate their recyclability. It was observed that both the catalysts efficiently reduce 4-NP up to 13 catalytic cycles without significant loss in its activity. The bar diagram for reduction time taken for each cycle is shown in **Figure 2.18 (A)**. Further, the catalysts were characterized after 13^{th} catalytic cycle using FTIR, HRTEM and XPS**.** FTIR revealed the appearance of new band in 500-560 cm^{-1} corresponding of the Fe-O which occurred due to surface oxidation of nZVI **(Figure 2.18 (B))**.

The agglomeration of nZVI after 13th catalytic cycle was observed from HRTEM analysis which can result in the loss of the catalytic activity **(Figure 2.18 (C)).** The XPS spectrum of the recycled CDLA@nZVI catalyst after 13th catalytic cycles showed the absence of shoulder peak of Fe^0 which suggests the slow oxidation of zerovalent iron nanoparticles **(Figure 2.18 (D)).** The analysis result of the recycled catalysts revealed that both the catalysts before and after the reaction cycles were mainly composed of the elements Fe, C and O which is consistent with the EDX mapping result. At the same time, the higher affinities of the crosslinked polymers towards the Fe NPs were beneficial to the recycling performance of both the catalysts.

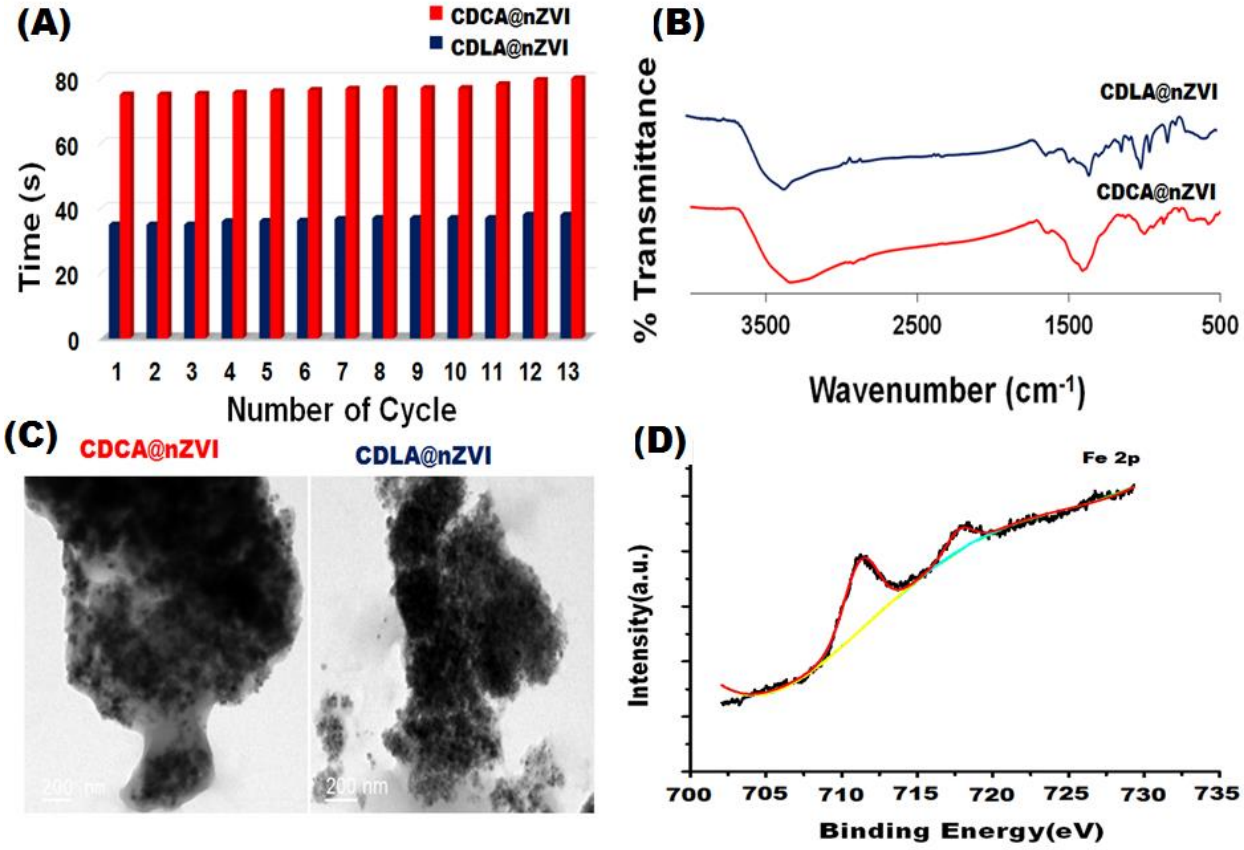

Figure 2.18: Analysis of (A) recyclability of CDLA@nZVI and CDCA@nZVI; Characterization of the recycled catalyst via (B) FTIR (C) HRTEM and (D) XPS techniques.

2.3.8 Proposed mechanism for reduction of nitroaromatics

The plausible mechanism for the catalytic reduction of nitrophenol molecules using both CDCA@nZVI and CDLA@nZVI has been illustrated in **Figure 2.19**.

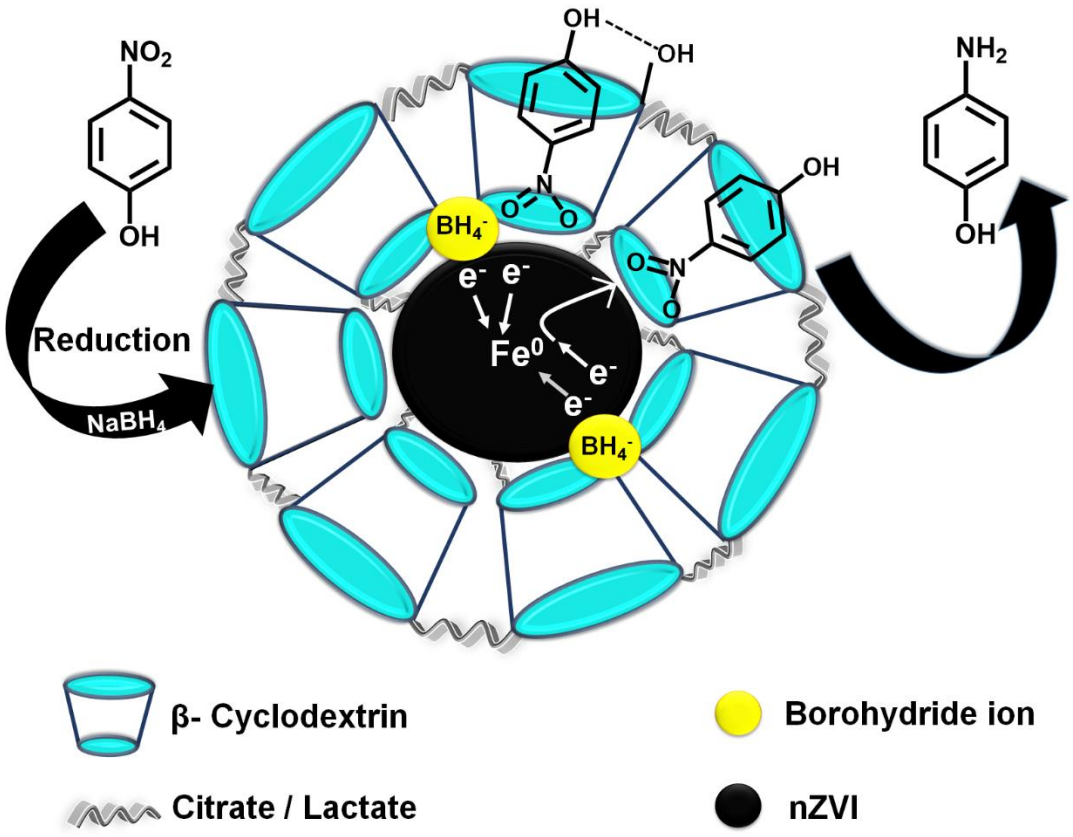

Figure 2.19: Schematic showing a probable mechanism for catalyzing the reduction of p-nitrophenol using citrate/lactate modified cyclodextrin capped nZVI Nanocatalyst

Zerovalent iron nanoparticles and sodium borohydride can act as the catalytic system, where the electrons were transferred from the donor nucleophile BH_4^- to the acceptor nitro group[34]. It is also known that sodium borohydride can generate borohydride anions in aqueous solution[49].

The process of adsorption of reactant and surface hydrogen species derived for borohydride onto the surface of the metal nanoparticles is rapid and reversible which can be described in terms of Langmuir isotherms[1]. In the sonochemical catalytic reduction the adsorption of BH_4^- on the surface of the nZVI may form a metal hydride complex as a reactive intermediate, which would aid in new surface sites with a high reductive ability[34]. It is well documented in the literature that nZVI have capability to react with water quickly and produce primary reaction intermediate

(HFeOH), which act as crucial reductant for the reaction in water[50].

Capping zerovalent Fe nanoparticles by crosslinked polymer derived from modified β-CD provides a platform for host guest interactions. Introducing β-CD molecules to the system, facilitates a supramolecular host which due to its amphiphilic nature can cap the FeNPs and also plays the role for the inclusion of substrate in the catalyst[51], [52],[53]. The driving force for the formation of this inclusion complex is hydrogen bonding with β-CD hydroxy groups which is also reversible. This means that the guest molecule can leave the hydrophobic inner cavity of β-CD after completion of the reaction. The inclusion complex formed by substrates in the β-CD cavities facilitated the reduction of 4-NP by electron transfer from the FeNPs core. This structural setup leads to increased entrapment of substrate molecules, subsequently increasing the electron transfer between nitrophenol molecule and $NaBH_4$ on the metal surface. This in turn leads to the reduction of the activation energy. The reaction is also accelerated due to the increased collisions between reactants as a result of vibration and turbulences rising from the cavitation phenomenon[22]. The physical effects of ultrasonication includes an increase in temperature, effective mass transfer through turbulent mixing and acoustic streaming which aid in enhancing the rate of reaction in aqueous medium[54]. The outcomes such as fast conversion, reduced reaction time are due to the synergistic effect of the catalysts and ultrasonication.

2.4 Conclusion

This chapter reports the synthesis of sustainable citric acid and lactic acid crosslinked cyclodextrin polymers via a simple one-pot esterification reaction for capping for zerovalent iron nanoparticles via ultrasonication method. The sonochemical approach imparted a good control over the morphology, nano size and dispersibility of the prepared FeNPs. The synthesized polymer capped nZVI catalysed the sonochemical conversion of 4-nitrophenol to 4-aminophenol in a very short time in aqueous medium. Application of the ultrasonication to the reaction system increases the temperature and reduced the reaction time. In addition, the surface area of nZVI was increased. Several other nitroaromatic compounds could be reduced with excellent isolated yield (89–95%), as well as high TON and TOF. According to proposed mechanism, the synergistic effect of substrate captured in cyclodextrin cavity, the subsequent electron donation from metallic core and sonochemical effect facilitates a rapid conversion of the reactants in aqueous media. The recycling studies especially revealed the robust nature of the polymer capped nZVI. The rate constant values

obtained from kinetic studies suggested that the catalytic activity of nZVI is comparable to the commonly used noble metal catalysts.

2.5 References

[1] P. Nariya, M. Das, F. Shukla, S. Thakore, Synthesis of magnetic silver cyclodextrin nanocomposite as catalyst for reduction of nitro aromatics and organic dyes, J. Mol. Liq. 300 (2020) 112279. https://doi.org/10.1016/j.molliq.2019.112279.

[2] K. Bhaduri, B.D. Das, R. Kumar, S. Mondal, S. Chatterjee, S. Shah, J.J. Bravo-Suárez, B. Chowdhury, Recyclable Au/SiO 2 -Shell/Fe 3 O 4 -Core Catalyst for the Reduction of Nitro Aromatic Compounds in Aqueous Solution, ACS Omega. 4 (2019) 4071–4081. https://doi.org/10.1021/acsomega.8b03655.

[3] H.F. Chen, M.J. Hung, T.H. Hung, Y.W. Tsai, C.W. Su, J. Yang, G.G. Huang, Single-Step Preparation of Silver-Doped Magnetic Hybrid Nanoparticles for the Catalytic Reduction of Nitroarenes, ACS Omega. 3 (2018) 3340–3347. https://doi.org/10.1021/acsomega.7b01987.

[4] A. Fürstner, Iron catalysis in organic synthesis: A critical assessment of what it takes to make this base metal a multitasking champion, ACS Cent. Sci. 2 (2016) 778–789. https://doi.org/10.1021/acscentsci.6b00272.

[5] S.R. Mofradnia, R. Ashouri, Z. Tavakoli, F. Shahmoradi, H. Rashedi, F. Yazdian, Effect of zero-valent iron/starch nanoparticle on nitrate removal using MD simulation, Int. J. Biol. Macromol. 121 (2019) 727–733. https://doi.org/10.1016/j.ijbiomac.2018.09.183.

[6] Y. Monga, P. Kumar, R.K. Sharma, J. Filip, R.S. Varma, R. Zbořil, M.B. Gawande, Sustainable Synthesis of Nanoscale Zerovalent Iron Particles for Environmental Remediation, ChemSusChem. 13 (2020) 3288–3305. https://doi.org/10.1002/cssc.202000290.

[7] K. Sravanthi, D. Ayodhya, P.Y. Swamy, Materials Science for Energy Technologies Green synthesis , characterization and catalytic activity of 4-nitrophenol reduction and formation of benzimidazoles using bentonite supported zero valent iron nanoparticles, Mater. Sci. Energy Technol. 2 (2019) 298–307.

https://doi.org/10.1016/j.mset.2019.02.003.

[8] K. Krawczyk, S. Wacławek, D. Silvestri, V.V.T. Padil, M. Řezanka, M. Černík, M. Jaroniec, Surface modification of zero-valent iron nanoparticles with β-cyclodextrin for 4-nitrophenol conversion, J. Colloid Interface Sci. 586 (2021) 655–662. https://doi.org/10.1016/j.jcis.2020.10.135.

[9] K.A.H.S. Sewwandi, R. Nitisoravut, Nano zero valent iron embedded on chitosan for enhancement of biohydrogen production in dark fermentation, Energy Reports. 6 (2020) 392–396. https://doi.org/10.1016/j.egyr.2020.11.225.

[10] J. Okuo, A. Emina, S. Omorogbe, B. Anegbe, Synthesis, characterization and application of starch stabilized zerovalent iron nanoparticles in the remediation of Pb-acid battery soil, Environ. Nanotechnology, Monit. Manag. 9 (2018) 12–17. https://doi.org/10.1016/j.enmm.2017.11.004.

[11] N. Bossa, A.W. Carpenter, N. Kumar, C.F. De Lannoy, M. Wiesner, Cellulose nanocrystal zero-valent iron nanocomposites for groundwater remediation, Environ. Sci. Nano. 4 (2017) 1294–1303. https://doi.org/10.1039/c6en00572a.

[12] S. Eslami, M.A. Ebrahimzadeh, P. Biparva, Green synthesis of safe zero valent iron nanoparticles by: Myrtus communis leaf extract as an effective agent for reducing excessive iron in iron-overloaded mice, a thalassemia model, RSC Adv. 8 (2018) 26144–26155. https://doi.org/10.1039/c8ra04451a.

[13] S. Bae, W. Lee, Influence of riboflavin on nanoscale zero-valent iron reactivity during the degradation of carbon tetrachloride, Environ. Sci. Technol. 48 (2014) 2368–2376. https://doi.org/10.1021/es4056565.

[14] J. Gong, C.S. Lee, E.J. Kim, Y.Y. Chang, Y.S. Chang, Enhancing the reactivity of bimetallic Bi/Fe0 by citric acid for remediation of polluted water, J. Hazard. Mater. 310 (2016) 135–142. https://doi.org/10.1016/j.jhazmat.2016.02.027.

[15] J. Yan, L. Han, W. Gao, S. Xue, M. Chen, Biochar supported nanoscale zerovalent iron composite used as persulfate activator for removing trichloroethylene, Bioresour. Technol. 175 (2015) 269–274. https://doi.org/10.1016/j.biortech.2014.10.103.

[16] S. Wang, B. Gao, Y. Li, A.E. Creamer, F. He, Adsorptive removal of arsenate from aqueous solutions by biochar supported zero-valent iron nanocomposite: Batch and continuous flow tests, J. Hazard. Mater. 322 (2017) 172–181. https://doi.org/10.1016/j.jhazmat.2016.01.052.

[17] W. Teng, J. Fan, W. Wang, N. Bai, R. Liu, Y. Liu, Y. Deng, B. Kong, J. Yang, D. Zhao, W. xian Zhang, Nanoscale zero-valent iron in mesoporous carbon (nZVI@C): stable nanoparticles for metal extraction and catalysis, J. Mater. Chem. A. 5 (2017) 4478–4485. https://doi.org/10.1039/c6ta10007d.

[18] A. Soliemanzadeh, M. Fekri, The application of green tea extract to prepare bentonite-supported nanoscale zero-valent iron and its performance on removal of Cr(VI): Effect of relative parameters and soil experiments, Microporous Mesoporous Mater. 239 (2017) 60–69. https://doi.org/10.1016/j.micromeso.2016.09.050.

[19] Z.X. Chen, X.Y. Jin, Z. Chen, M. Megharaj, R. Naidu, Removal of methyl orange from aqueous solution using bentonite-supported nanoscale zero-valent iron, J. Colloid Interface Sci. 363 (2011) 601–607. https://doi.org/10.1016/j.jcis.2011.07.057.

[20] Z. Yuan, H. Liu, H. Wu, Y. Wang, Q. Liu, Y. Wang, S.F. Lincoln, X. Guo, J. Wang, Cyclodextrin Hydrogels: Rapid Removal of Aromatic Micropollutants and Adsorption Mechanisms, J. Chem. Eng. Data. 65 (2020) 678–689. https://doi.org/10.1021/acs.jced.9b00913.

[21] M. Das, A. Solanki, A. Joshi, R. Devkar, S. Seshadri, S. Thakore, B-Cyclodextrin Based Dual-Responsive Multifunctional Nanotheranostics for Cancer Cell Targeting and Dual Drug Delivery, Carbohydr. Polym. 206 (2019) 694–705. https://doi.org/10.1016/j.carbpol.2018.11.049.

[22] G. Chatel, Sonochemistry in nanocatalysis: the use of ultrasound from the catalyst synthesis to the catalytic reaction, Curr. Opin. Green Sustain. Chem. (2018). https://doi.org/10.1016/j.cogsc.2018.07.004.

[23] H. Ullah, I. Khan, Z.H. Yamani, A. Qurashi, Sonochemical-driven ultrafast facile synthesis of SnO2 nanoparticles: Growth mechanism structural electrical and hydrogen gas sensing properties, Ultrason. Sonochem. 34 (2017) 484–490.

https://doi.org/10.1016/j.ultsonch.2016.06.025.

[24] J. Balachandramohan, T. Sivasankar, Ultrasound assisted synthesis of guar gum-zero valent iron nanocomposites as a novel catalyst for the treatment of pollutants, Carbohydr. Polym. 199 (2018) 41–50. https://doi.org/10.1016/j.carbpol.2018.06.097.

[25] K.K.R. Datta, E. Petala, K.J. Datta, J.A. Perman, J. Tucek, P. Bartak, M. Otyepka, G. Zoppellaro, R. Zboril, StereoselectiveNZVI modified magnetic filter paper with high redox and catalytic activities for advanced water treatment technologies, Chem. Commun. 50 (2014) 15673–15676. https://doi.org/10.1039/c4cc06241h.

[26] F. Shukla, M. Das, S. Thakore, Copper nanoparticles loaded polymer vesicles as environmentally amicable nanoreactors: A sustainable approach for cascading synthesis of benzimidazole, J. Mol. Liq. 336 (2021) 116217. https://doi.org/10.1016/j.molliq.2021.116217.

[27] M. Yadav, M. Das, C. Savani, S. Thakore, R. Jadeja, Maleic Anhydride Cross-Linked β-Cyclodextrin-Conjugated Magnetic Nanoadsorbent: An Ecofriendly Approach for Simultaneous Adsorption of Hydrophilic and Hydrophobic Dyes, ACS Omega. 4 (2019) 11993–12003. https://doi.org/10.1021/acsomega.9b00881.

[28] M. Sundarapandi, P. Viswanathan, S. Sivakumar, R. Ramaraj, Catalytic Activities of Mono- and Bimetallic (Gold/Silver) Nanoshell-Coated Gold Nanocubes toward Catalytic Reduction of Nitroaromatics, Langmuir. 34 (2018) 13897–13904. https://doi.org/10.1021/acs.langmuir.8b02096.

[29] H. Veisi, Z. Joshani, B. Karmakar, T. Tamoradi, M.M. Heravi, J. Gholami, Ultrasound assisted synthesis of Pd NPs decorated chitosan-starch functionalized Fe3O4 nanocomposite catalyst towards Suzuki-Miyaura coupling and reduction of 4-nitrophenol, Int. J. Biol. Macromol. 172 (2021) 104–113. https://doi.org/10.1016/j.ijbiomac.2021.01.040.

[30] S. Kubendhiran, R. Sakthivel, S.M. Chen, B. Mutharani, T.W. Chen, Innovative Strategy Based on a Novel Carbon-Black-β-Cyclodextrin Nanocomposite for the Simultaneous Determination of the Anticancer Drug Flutamide and the Environmental Pollutant 4-Nitrophenol, Anal. Chem. 90 (2018) 6283–6291.

https://doi.org/10.1021/acs.analchem.8b00989.

[31] J.R. Deka, M.H. Lee, D. Saikia, H.M. Kao, Y.C. Yang, Confinement of Cu nanoparticles in the nanocages of large pore SBA-16 functionalized with carboxylic acid: Enhanced activity and improved durability for 4-nitrophenol reduction, Dalt. Trans. 48 (2019) 8227–8237. https://doi.org/10.1039/c9dt00248k.

[32] S. Chen, Y. Xiang, C. Peng, W. Xu, M.K. Banks, R. Wu, Synthesis of a novel graphene-based gold nanocomposite using PVEIM-: B -PNIPAM as a stabilizer and its thermosensitivity for the catalytic reduction of 4-nitrophenol, Inorg. Chem. Front. 6 (2019) 903–913. https://doi.org/10.1039/c8qi01303a.

[33] S. Bae, W. Lee, Inhibition of nZVI reactivity by magnetite during the reductive degradation of 1,1,1-TCA in nZVI/magnetite suspension, Appl. Catal. B Environ. 96 (2010) 10–17. https://doi.org/10.1016/j.apcatb.2010.01.028.

[34] D. Shi, G. Zhu, X. Zhang, X. Zhang, X. Li, J. Fan, Ultra-small and recyclable zero-valent iron nanoclusters for rapid and highly efficient catalytic reduction of p-nitrophenol in water, (2019) 1000–1010. https://doi.org/10.1039/c8nr08302a.

[35] K. Iqbal, A. Iqbal, A.M. Kirillov, C. Shan, W. Liu, Y. Tang, A new multicomponent CDs/Ag@Mg-Al-Ce-LDH nanocatalyst for highly efficient degradation of organic water pollutants, J. Mater. Chem. A. 6 (2018) 4515–4524. https://doi.org/10.1039/c8ta00258d.

[36] Q. Geng, J. Du, Reduction of 4-nitrophenol catalyzed by silver nanoparticles supported on polymer micelles and vesicles, RSC Adv. 4 (2014) 16425–16428. https://doi.org/10.1039/c4ra01866d.

[37] V.S. Ghorpade, A.V. Yadav, R.J. Dias, Citric acid crosslinked β-cyclodextrin/carboxymethylcellulose hydrogel films for controlled delivery of poorly soluble drugs, Carbohydr. Polym. (2017). https://doi.org/10.1016/j.carbpol.2017.02.005.

[38] R. Anand, M. Malanga, I. Manet, F. Manoli, K. Tuza, A. Aykaç, C. Ladavière, E. Fenyvesi, A. Vargas-Berenguel, R. Gref, S. Monti, Citric acid-γ-cyclodextrin crosslinked oligomers as carriers for doxorubicin delivery, Photochem. Photobiol. Sci. 12 (2013) 1841–1854. https://doi.org/10.1039/c3pp50169h.

[39] K.N. Jayaprabha, P.A. Joy, Citrate modified β-cyclodextrin functionalized magnetite nanoparticles: A biocompatible platform for hydrophobic drug delivery, RSC Adv. 5 (2015) 22117–22125. https://doi.org/10.1039/c4ra16044d.

[40] S. Zhu, S.H. Ho, X. Huang, D. Wang, F. Yang, L. Wang, C. Wang, X. Cao, F. Ma, Magnetic Nanoscale Zerovalent Iron Assisted Biochar: Interfacial Chemical Behaviors and Heavy Metals Remediation Performance, ACS Sustain. Chem. Eng. 5 (2017) 9673–9682. https://doi.org/10.1021/acssuschemeng.7b00542.

[41] A. Ghosh, S. Dutta, I. Mukherjee, S. Biswas, S. Chatterjee, R. Saha, Template-free synthesis of flower-shaped zero-valent iron nanoparticle: Role of hydroxyl group in controlling morphology and nitrate reduction, Adv. Powder Technol. 28 (2017) 2256–2264. https://doi.org/10.1016/j.apt.2017.06.006.

[42] J. Nasiri, E. Motamedi, M.R. Naghavi, M. Ghafoori, Removal of crystal violet from water using B-cyclodextrin functionalized biogenic zero-valent iron nanoadsorbents synthesized via aqueous root extracts of Ferula persica, J. Hazard. Mater. 367 (2019) 325–338. https://doi.org/10.1016/j.jhazmat.2018.12.079.

[43] T. Wen, X. Wang, J. Wang, Z. Chen, J. Li, J. Hu, T. Hayat, A. Alsaedi, B. Grambow, X. Wang, A strategically designed porous magnetic N-doped Fe/Fe3C@C matrix and its highly efficient uranium(VI) remediation, Inorg. Chem. Front. 3 (2016) 1227–1235. https://doi.org/10.1039/c6qi00091f.

[44] F. Paquin, J. Rivnay, A. Salleo, N. Stingelin, C. Silva, Multi-phase semicrystalline microstructures drive exciton dissociation in neat plastic semiconductors, Dalt. Trans. 3 (2015) 10715–10722. https://doi.org/10.1039/b000000x.

[45] Z.D. Ding, Y.X. Wang, S.F. Xi, Y. Li, Z. Li, X. Ren, Z.G. Gu, A Hexagonal Covalent Porphyrin Framework as an Efficient Support for Gold Nanoparticles toward Catalytic Reduction of 4-Nitrophenol, Chem. - A Eur. J. 22 (2016) 17029–17036. https://doi.org/10.1002/chem.201603212.

[46] V.K. Harika, H.K. Sadhanala, I. Perelshtein, A. Gedanken, Sonication-Assisted Synthesis of Bimetallic Hg/Pd Alloy Nanoparticles for Catalytic Reduction of Nitrophenol and its Derivatives, Ultrason. Sonochem. 60 (2020) 104804.

https://doi.org/10.1016/j.ultsonch.2019.104804.

[47] M. Serhan, M. Sprowls, D. Jackemeyer, M. Long, I.D. Perez, W. Maret, N. Tao, E. Forzani, Preparation of Hollow Fe3O4/Pd@C NCs to stabilize subminiature Pd nanoparticles for reduction of 4-nitrophenol, AIChE Annu. Meet. Conf. Proc. 2019-Novem (2019). https://doi.org/10.1039/x0xx00000x.

[48] X. Cui, Y. Zheng, M. Tian, Z. Dong, Novel yolk–shell-structured Fe 3 O 4 @γ-AlOOH nanocomposite modified with Pd nanoparticles as a recyclable catalyst with excellent catalytic activity, Appl. Surf. Sci. 416 (2017) 103–111. https://doi.org/10.1016/j.apsusc.2017.04.048.

[49] H.J. Lu, J.K. Wang, S. Ferguson, T. Wang, Y. Bao, H.X. Hao, Mechanism, synthesis and modification of nano zerovalent iron in water treatment, Nanoscale. 8 (2016) 9962–9975. https://doi.org/10.1039/c6nr00740f.

[50] Q. Li, Z. Chen, H. Wang, H. Yang, T. Wen, S. Wang, B. Hu, X. Wang, Removal of organic compounds by nanoscale zero-valent iron and its composites, Sci. Total Environ. 792 (2021) 148546. https://doi.org/10.1016/j.scitotenv.2021.148546.

[51] M. Yadav, M. Das, S. Bhatt, P. Shah, R. Jadeja, S. Thakore, Rapid selective optical detection of sulfur containing agrochemicals and amino acid by functionalized cyclodextrin polymer derived gold nanoprobes, Microchem. J. 169 (2021) 106630. https://doi.org/10.1016/j.microc.2021.106630.

[52] A. Zare Asadabadi, S.J. Hoseini, M. Bahrami, S.M. Nabavizadeh, Catalytic applications of β-cyclodextrin/palladium nanoparticle thin film obtained from oil/water interface in the reduction of toxic nitrophenol compounds and the degradation of azo dyes, New J. Chem. 43 (2019) 6513–6522. https://doi.org/10.1039/c8nj06449k.

[53] B. Qi, C. Wu, Y. Liu, J. Liu, H. Zhang, Self-Assembled Magnetic Pt Nanocomposites for the Catalytic Reduction of Nitrophenol, ACS Appl. Nano Mater. 2 (2019) 4377–4385. https://doi.org/10.1021/acsanm.9b00794.

[54] D.S. Patle, S. Sharma, A.P. Gadhamsetti, K.R. Balinge, P.R. Bhagat, S. Pandit, S. Kumar, Ultrasonication-Assisted and Benzimidazolium-Based Brønsted Acid Ionic Liquid-

Catalyzed Transesterification of Castor Oil, ACS Omega. 3 (2018) 15455–15463. https://doi.org/10.1021/acsomega.8b02021.

Spectral data

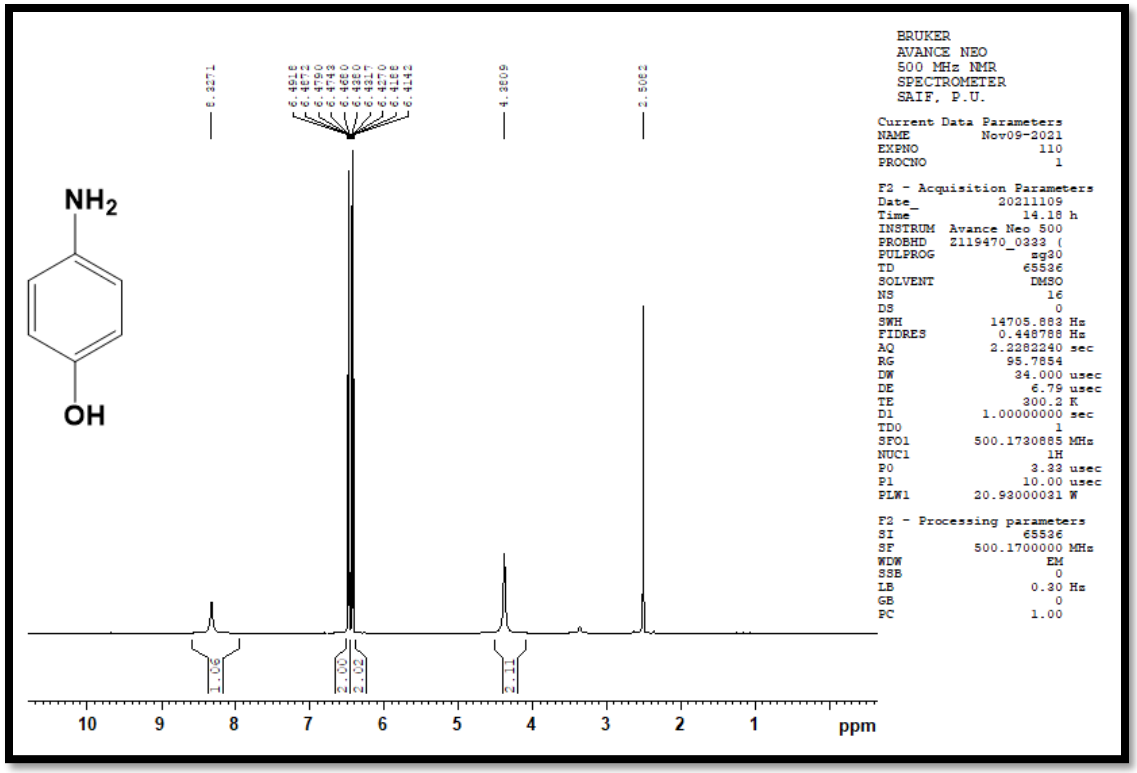

Figure S1: ^{1}H NMR of 4-Aminophenol

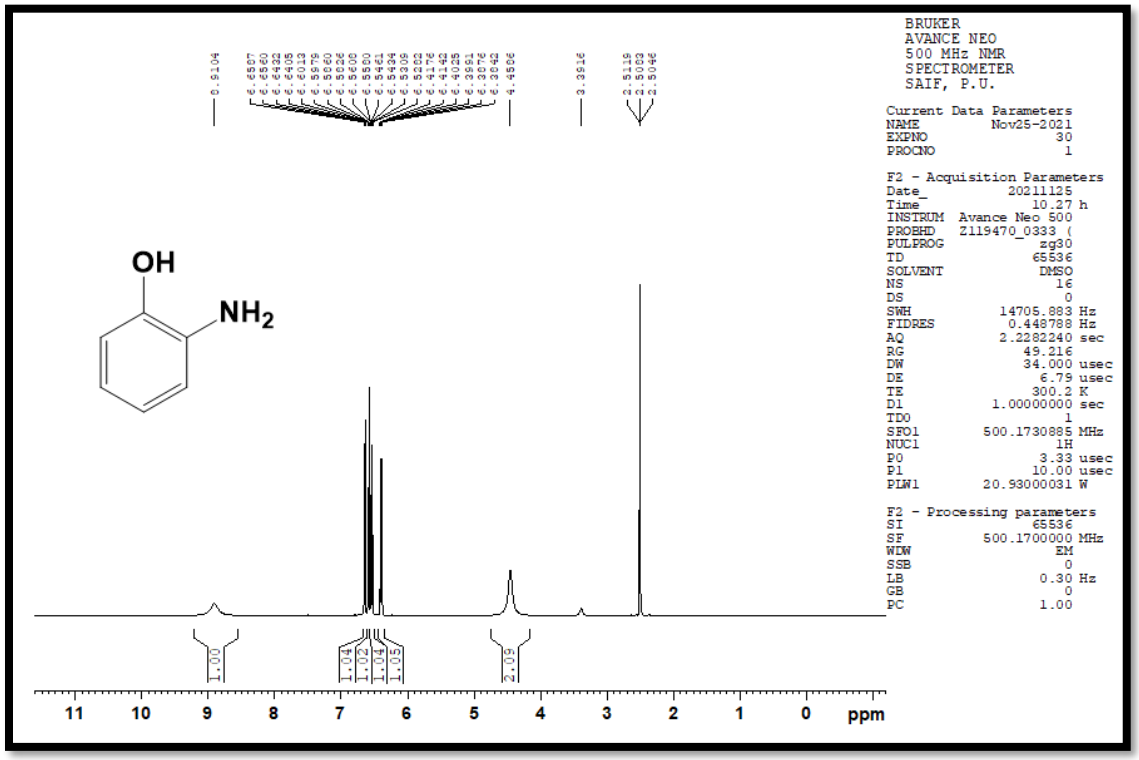

Figure S2: ^{1}H NMR of 2-Aminophenol

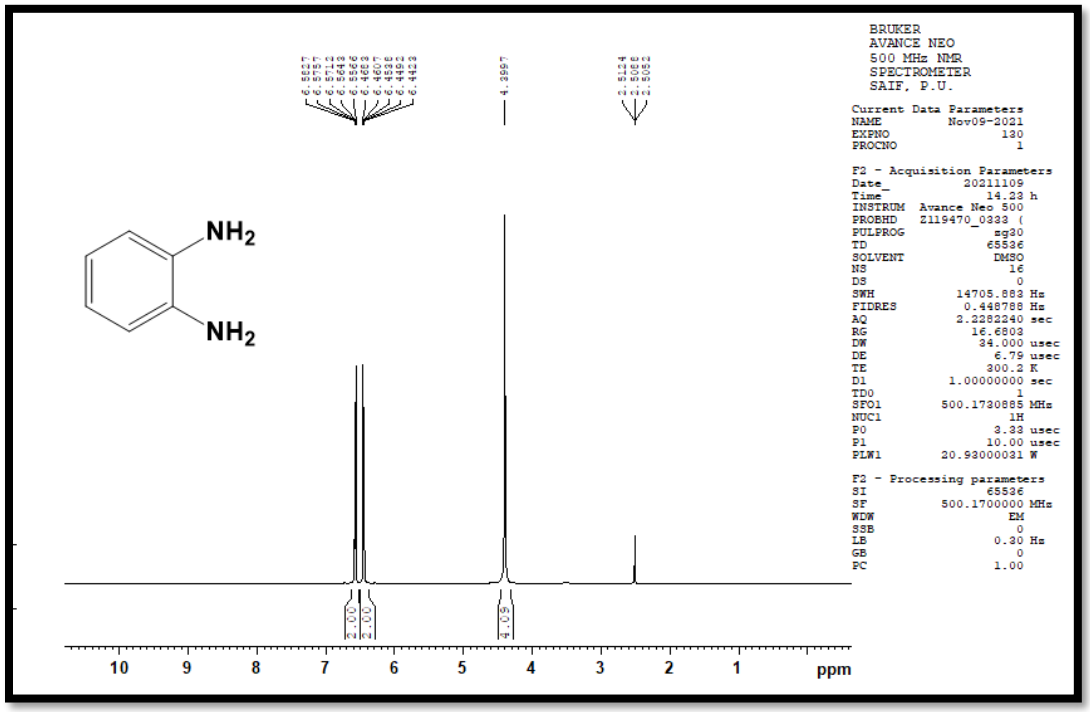

Figure S3: ^{1}H NMR of o-phenylenediamine

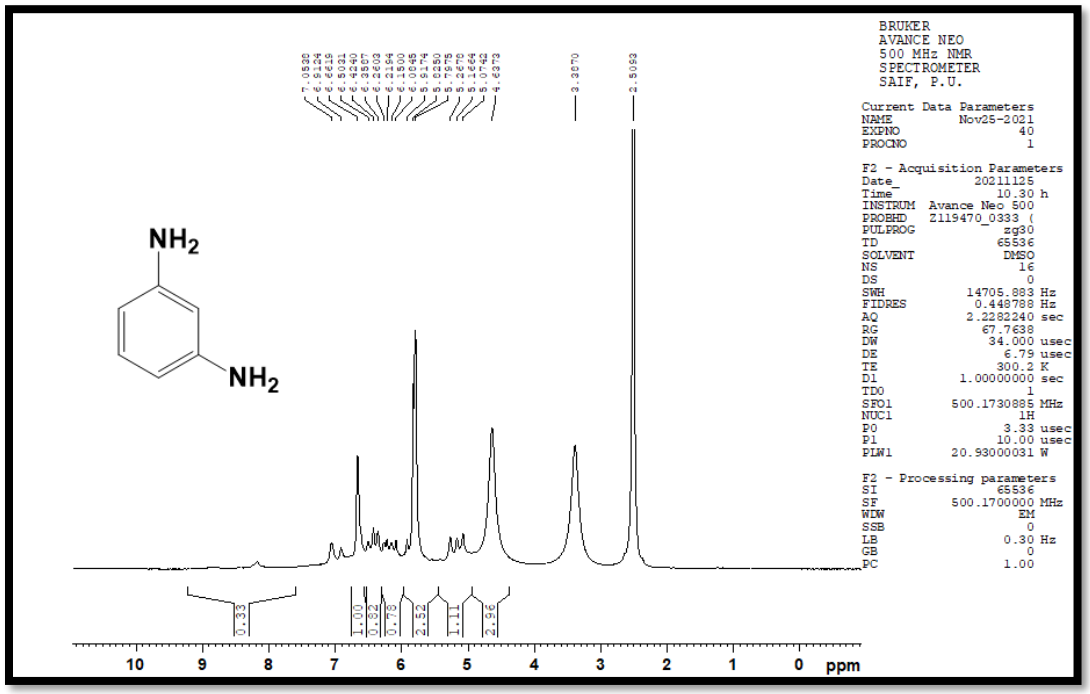

Figure S4: ^{1}H NMR of m-phenylenediamine

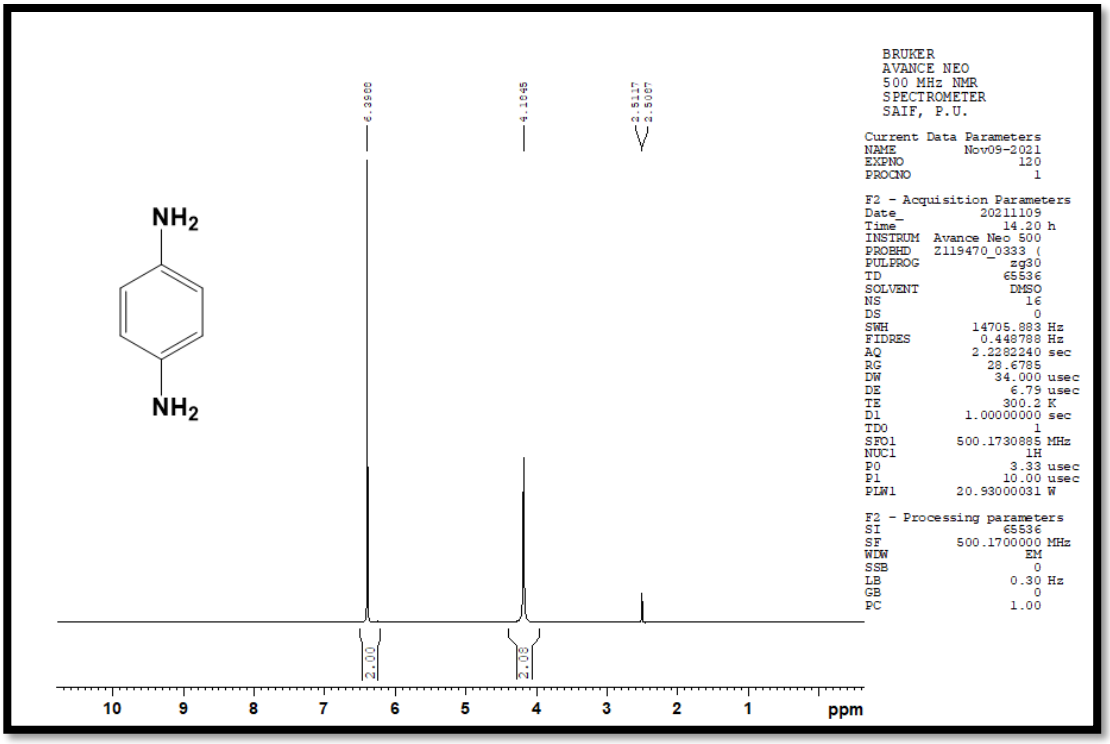

Figure S5: ^{1}H NMR of p-phenylenediamine

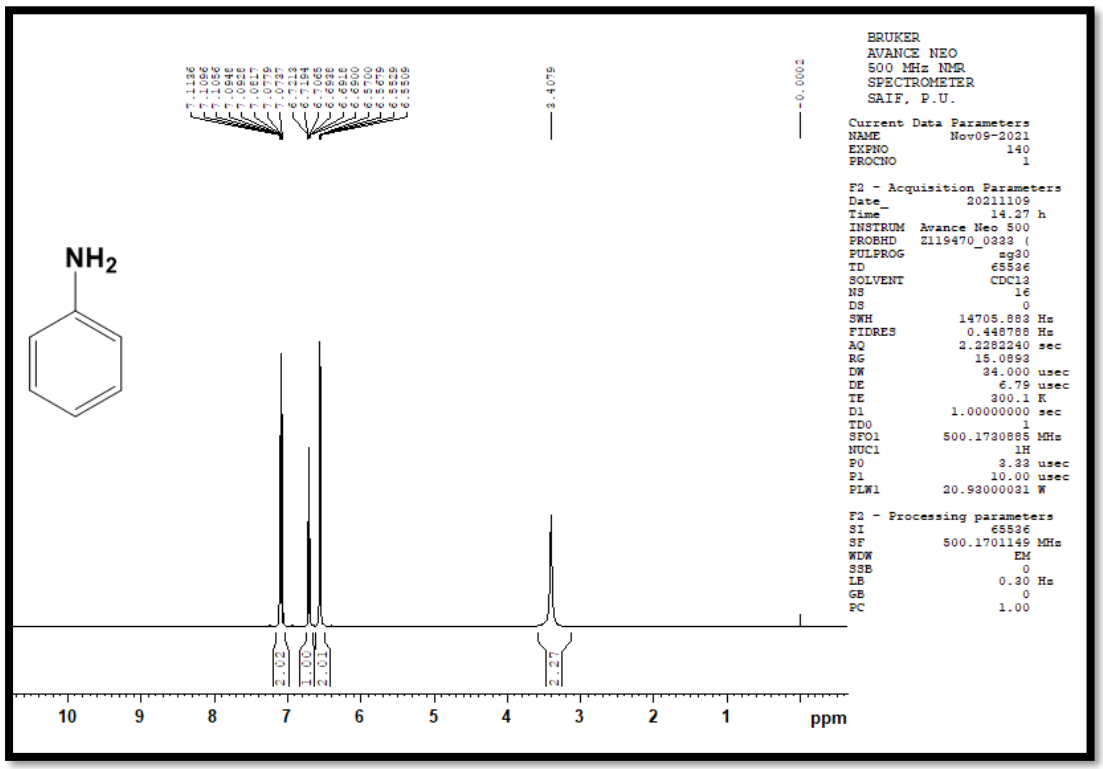

Figure S6: ^{1}H NMR of Aniline